



Review

Self-Assembly in Polyoxometalate and Metal Coordination-Based Systems: Synthetic Approaches and Developments

Stamatis Passadis ¹, Themistoklis A. Kabanos ^{1,*}, Yu-Fei Song ^{2,*} and Haralampos N. Miras ^{3,*}

¹ Section of Inorganic and Analytical Chemistry, Department of Chemistry, University of Ioannina, 45110 Ioannina, Greece; stamatispassadis@hotmail.com

² Beijing Advanced Innovation Center for Soft Matter Science and Engineering, State Key Laboratory of Chemical Resource Engineering, Beijing University of Chemical Technology, Beijing 100029, China

³ WestCHEM, School of Chemistry, University of Glasgow, University Avenue, Glasgow G12 8QQ, UK

* Correspondence: tkampano@cc.uoi.gr (T.A.K.); songyf@mail.buct.edu.cn (Y.-F.S.); charalampos.moiras@glasgow.ac.uk (H.N.M.); Tel.: +44-141-330-4375 (H.N.M)

Received: 8 June 2018; Accepted: 9 July 2018; Published: 13 July 2018



Abstract: Utilizing new experimental approaches and gradual understanding of the underlying chemical processes has led to advances in the self-assembly of inorganic and metal–organic compounds at a very fast pace over the last decades. Exploitation of unveiled information originating from initial experimental observations has sparked the development of new families of compounds with unique structural characteristics and functionalities. The main source of inspiration for numerous research groups originated from the implementation of the design element along with the discovery of new chemical components which can self-assemble into complex structures with wide range of sizes, topologies and functionalities. Not only do self-assembled inorganic and metal–organic chemical systems belong to families of compounds with configurable structures, but also have a vast array of physical properties which reflect the chemical information stored in the various “modular” molecular subunits. The purpose of this short review article is not the exhaustive discussion of the broad field of inorganic and metal–organic chemical systems, but the discussion of some representative examples from each category which demonstrate the implementation of new synthetic approaches and design principles.

Keywords: self-assembly; supramolecular chemistry; coordination chemistry; polyoxometalates; metal–organic frameworks; clusters

1. Introduction

The term self-assembly is frequently used to describe an extended network of equilibria which can be exploited in synthetic chemistry in order to construct complex molecular structures from molecular synthons linked by covalent bonds. This area of research is governed by a specific set of rules which has attracted the interest of numerous research groups over the last decades. On the other hand, the supramolecular chemistry aspect is considered a complementary research area and extends beyond the molecular chemistry, has also attracted substantial interest and is responsible for the formation of chemical systems using building blocks of appropriate structural features and chemical properties interacting via non-covalent intermolecular forces. The first signs of this new field emerged in 1967 by the work of Jean-Marie Lehn in the design and study of alkali-metal cryptates, and the identification of the phenomenon of molecular recognition in chemical systems. This initial observation set the scene for the development of the field of supramolecular chemistry [1] and resulted in the award of the Nobel Prize in chemistry in 1987. Supramolecular chemistry investigates the interactions between molecular

species and aims to shed light upon the underlying mechanisms which lead to the construction of highly complicated and functional chemical systems, constructed by constituents which are held by or temporarily interact with intermolecular bonds. Due to the instability of the non-covalent interactions, the available molecular synthons can connect and disconnect reversibly, by rearranging and re-organizing their components [2]. In other words, depending on a wide range of experimental and chemical stimuli, they can self-organize spontaneously via the process of self-assembly into well-defined supramolecular architectures. Self-assembly processes and supramolecular interactions have been identified as the main driving forces responsible for the formation and ultimately for the observed functionality of a wide range of chemical systems. Thus, we will focus our discussion on a subset of inorganic and metal–organic systems and more specifically in polyoxometalates, metal–organic frameworks (MOFs) and metal coordination cages.

The process of self-organization is generally considered to proceed over three stages: (1) molecular recognition; (2) growth through the connection of multiple constituents; (3) termination, where the process is completed [3]. A representative example of this process can be in polyoxometalate systems, which can lead to the formation of a wide range of intricate and functional architectures. For example, the self-assembly process is responsible for the formation of the family of molybdenum blue nano-sized clusters, such as the wheel-shaped $\{Mo_{154}\}$ oxide cluster where intermolecular interactions can promote the formation of vesicles depending on the experimental conditions [4]. The formation of polyoxometalate-based vesicles is the result of a delicate balance between short-range attractive Van der Waals forces, hydrogen bond forces, and repulsive electrostatic interactions between the anionic clusters. As we mentioned earlier, the self-assembly process depends on a wide range of external parameters (pH, concentration, ligands, templates, temperature, pressure, etc.); even small variations of these parameters can affect the complex network of equilibria established initially in the reaction mixture and consequently trigger the formation of different species in solution. Muller et al. reported that the $\{Mo_{72}Fe_{30}\}$ clusters in dilute aqueous solution behave as nano-sized weak inorganic acids and can be deprotonated, according to the pH, which leads to the formation of different size molecular nanoobjects (Figure 1) [5].

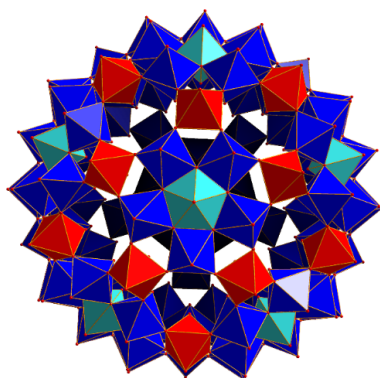


Figure 1. Structure of the spherical $\{Mo_{72}Fe_{30}\}$ Keplerate cluster. Mo, Blue and light blue polyhedral; Fe, red polyhedral; Oxygen, red spheres.

The self-assembly process is usually system-specific, which makes our efforts to unveil the underlying reactions and understand better the overall process extremely challenging. Apart from the experimental approaches which occasionally involve real time monitoring of chemical reactions and identification of short-lived intermediate species [6–8], theoretical calculations and simulation models also make it possible, in some cases, to extract crucial mechanistic information. Fujita et al. reported the simulation of the formation process of the M_6L_8 coordination cage ($M = Pd(II)$ and $L =$ pyridine-capped tridentate ligands) in 3 stages (assembly, evolution, fixation), which is in agreement with the experimental data [9]. The authors showed that the life time of the coordinatively unsaturated

intermediate species play a key role in the self-assembly process of the final complete M_6L_8 cage. Recently, the same group implemented the same simulation model to predict the formation of the larger $M_{12}L_{24}$ cage ($M = Pd(II)$ and $L =$ pyridine-capped bidentate ligands) following a similar approach (Figure 2) [10]. In this case, the self-assembly process revealed the existence of kinetically trapped structures of lower nuclearity, while the observed behaviour depends on geometrical parameters such as the bond angle of the ligands as well as the strength of the metal–ligand bond. This is a very important observation, which needs to be taken into consideration when trying to understand the underlying processes that govern the formation of large clusters. Very often, kinetic effects make prediction of self-assembled structures of higher nuclearity clusters extremely challenging.

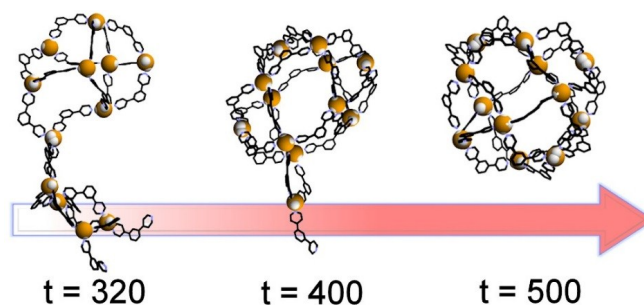


Figure 2. Structural changes during the self-assembly process. Adapted from *ACS Nano* 2014, 8(2), 1290–1296. Copyright (2014) American Chemical Society.

Identification of intermediate species masked by the self-assembly processes during the “one-pot” reaction is crucial for the understanding of the formation mechanism. Recently, Cronin et al., reported an alternative approach by employing a synthetic process under continuous flow conditions for the investigation of self-assembly driven formation of molybdenum blue nanoclusters. The concurrent control of four experimental variables (pH, Mo concentration, reducing agent, flow rate) kept the system far from equilibrium for a given period of time which proved to be crucial for the identification and isolation of the intermediate species [11]. In this case, it was concluded that the formation mechanism of the $\{Mo_{(154-x)}\}$ family involves the $\{Mo_{36}\}$ cluster which acts as a structure-directing template (Figure 3). The more we understand the mechanism behind the self-assembly processes, the more constructive will be the implementation of a design element which will allow the construction of chemical systems with intricate structures, unique properties and a large range of applications.

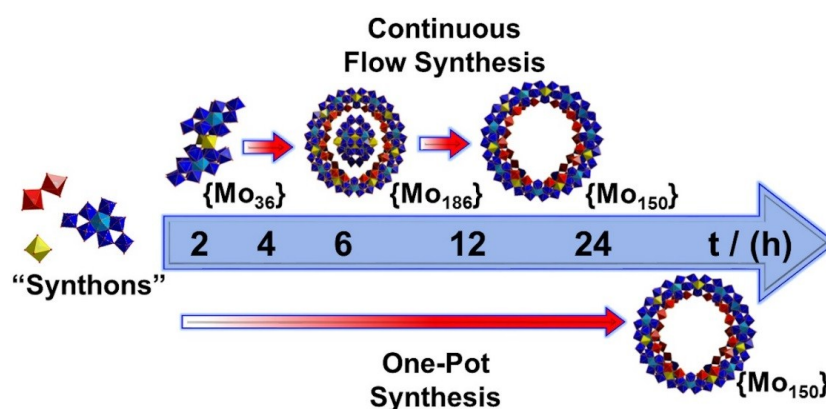


Figure 3. Formation of $\{Mo_{186}\}$, $\{Mo_{150}\}$ and $\{Mo_{36}\}$ complexes. The flow-reaction conditions and the reducing environment are necessary factors for the isolation of $\{Mo_{36}\}$. Colour scheme, yellow: $\{Mo_1\}$, red; $\{Mo_2\}$, blue; $\{Mo_8\}$.

2. Polyoxometalate Systems

2.1. POM-Based Clusters and Supramolecular Aggregates

Polyoxometalates are a class of discrete molecular inorganic clusters also known as polyoxoanions or polyanions. These are formed by metals (addenda atoms) such as tungsten, molybdenum and vanadium in their higher oxidation state; however, over the last decades, it has been shown that other metals can serve as the primary atoms within POM clusters, such as niobium [12,13], and tantalum [14,15]. POMs are composed of condensed metal-oxygen $\{MO_x\}$ polyhedra ($x = 4$ to 7). POMs can be formed mainly by vanadium, molybdenum and tungsten due to their appropriate ionic size and their ability to act as good acceptors of oxygen's π electrons. The fundamental requirements for a transition metal to serve as addenda are the ability to adopt a variety of coordination modes (mainly 4 to 6) in response to acidification, have high positive charge, and are capable of $p\pi$ - $d\pi$ interactions. However, there are a few examples that deviate from this set of rules, as reported by Kortz et al., where the authors demonstrated the preparation and characterization of metal oxides made of noble metals such as Au [16,17] and Pd [18–22] in the presence of supporting organic or inorganic ligands.

There are a number of archetypal POMs that are well documented in the literature and many other POMs contain structural features of these “classical” architectures. Such architectures are dominant in the field because of their high reproducibility, stability and the fact that they can be formed using several different types of addenda metal atoms. They can also incorporate a wide range of heteroatoms and still maintain their structure, a feature not present in most examples of polyoxometalates. The classical POMs are often used as starting materials for the construction of larger structures or for the manufacturing of POM-based materials due to their stability under specific experimental conditions. POM clusters can be classified in three general categories [23–25]; (1) heteropolyanions are the most explored category, and they consist of metal-oxide clusters of Mo, W, V, which contain XO_4^{n-} type heteroanions, where $X = B, Si, Ge, P,$ and S . Heteroanions induce stability to the clusters as well as to their lacunary derivatives generated by the removal of one or more addenda atoms. In the first category for example, belong the two well-known POM archetypes, Keggin and Dawson. The Keggin structure $[(XO_4)_4M_{12}O_{36}]^{n-}$ ($M = Mo, W; X = S, P, Si,$ et al.), which was confirmed in 1933, consists of $\{MO_6\}$ octahedra connected to each other via edge sharing of oxygen ligands forming $\{M_3O_{13}\}$ triads, which are organised tetrahedrally around a central heteroatom. Similarly, the Dawson structure $[(XO_4)_2M_{18}O_{62}]^{n-}$ is the result of the assembly process of two lacunary Keggin monomers $[XM_6O_{34}]^{n-}$; (2) isopolyanions are POMs that are comprised entirely of addenda atoms. Typically, this means that only one type of metal is present; however, there are examples of mixed metal clusters where both metals are addenda and technically such clusters are also iso-POMs. Due to the lack of template heteroanion, isopolyanionic structures are less stable. An example for the second category is the Lindqvist anion $[M_6O_{19}]^{n-}$ ($M = W, Mo, V, Nb, Ta$), which is formed by 6 edge-sharing $\{MO_6\}$ octahedrals; (3) the Molybdenum Blues and Browns are the oldest class of POMs and were discovered by Scheele in 1793, but the structures could not be determined until the development of modern X-ray crystallographic analysis. They also represent the largest size of molecular POM clusters with some approaching the size of small proteins (the $\{Mo_{368}\}$ “blue lemon” is ~6 nm in diameter) [22]. Molybdenum Blues are defined by the fact that they contain mixed valence Mo^V/Mo^VI addenda and have delocalised electrons capable of intervalence charge transfer from Mo^V to Mo^VI facilitated by the π -orbitals of the bridging oxo ligands and this electronic interaction is responsible for their characteristic intense blue colour. Molybdenum Browns are further reduced comparing to Mo-Blues and have electrons localised between reduced Mo^V centres as $Mo-Mo$ bonds which contribute to the brown colour of these clusters. The reduction of molybdenum addenda is only possible for $\{O = MoO_5\}$ containing structures POMs. This is due to the fact that the molecular orbitals of $\{MOL_5\}$ complexes contain a non-bonding t_{2g} orbital capable of accepting electrons, while in *cis* $\{MO_2L_4\}$ complexes all the t_{2g} orbitals are associated with π -bonding to oxo ligands and as such there

are no available non-bonding orbitals for electrons to occupy and reduction would destabilise the clusters [26]. This rule induces certain constraints on the structural features of Molybdenum Blues and Browns. The most well-known Molybdenum Blue structures are the giant wheels, $\{\text{Mo}_{154}\}$ [27] and $\{\text{Mo}_{176}\}$ [28], and the $\{\text{Mo}_{132}\}$ Keplerate cluster [29], which are all constructed using the same structural building block, $\{\text{MoMo}_5\}$. The central building block is occupied by a pentagonal bipyramidal $\{\text{MoO}_7\}$ unit, which is surrounded by five edge-shared $\{\text{MoO}_6\}$ octahedra along the equator of the bipyramid. This pentagon is considered to be the fundamental unit responsible for the construction of elaborate architectures (see Figure 4). In wheel structures, the pentagonal building blocks are connected into ring architectures and are comprised of two such rings fused together. Each ring is formed from two distinct building blocks known as $\{\text{Mo}_8\}$ and $\{\text{Mo}_2\}$. The $\{\text{Mo}_8\}$ building block incorporates the pentagonal unit described previously with an additional two $\{\text{MoO}_6\}$ octahedra connected to the pentagon via corner sharing with four of the $\{\text{MoO}_6\}$ octahedra of the pentagonal unit. These additional molybdate units on the pentagon connect to neighbouring $\{\text{Mo}_8\}$ units via corner and edge sharing to produce the final ring-shaped structure. The rims of the wheel are supported by $\{\text{Mo}_2\}$ units, which consist of two corner-sharing $\{\text{MoO}_6\}$ octahedra. They connect to the $\{\text{Mo}_8\}$ building blocks via three sites of corner sharing. Two representative giant wheels— $\{\text{Mo}_{154}\}$, $[\text{Mo}_{154}\text{O}_{462}\text{H}_{14}(\text{H}_2\text{O})_{70}]^{14-}$ [27] and $\{\text{Mo}_{176}\}$, $[\text{Mo}_{176}\text{O}_{528}\text{H}_{16}(\text{H}_2\text{O})_{80}]^{16-}$ [28]—have external diameters of 3.4 and 4.1 nm, respectively. The $\{\text{Mo}_{176}\}$ has a smaller curvature because each ring possesses an additional $\{\text{Mo}_8\}$ building block relative to the $\{\text{Mo}_{154}\}$.



Figure 4. Ball-and-stick representation of the $\{\text{Mo}_6\}$ pentagonal bipyramidal building block integral to Molybdenum Blue and Brown architectures beside polyhedral and ball-and-stick representations of how the pentagonal units are arranged within the $\{\text{Mo}_{154}\}$ wheel and $\{\text{Mo}_{132}\}$ Keplerate. (Colour scheme: Mo, blue; O, red; the central Mo of the pentagonal units has been highlighted in pale blue).

Interestingly, POM-based structures such as Keggin, Dawson, Anderson, etc., can be used as secondary building blocks for the construction of larger architectures. There are many methods that can be used for the modification and functionalization of POM clusters, including the choice of counterions, organic ligands and transition metals. The counterions are necessary for the existence of POMs as they stabilize the negative charge, but they can also influence the self-assembly process during the formation of POM structures. Depending on their size, charge, solubility etc., can stabilize the intermediate building blocks and “transitional” species in solution, which ultimately influence the structural features of the final product [24]. The organic ligands and first row transition metals can be used as ligands and metal linkers. Additionally, the exchange of redox “innocent” templates (e.g., SO_4^{2-} and PO_4^{3-}) with redox active ones (e.g., SO_3^{2-} , SeO_3^{2-}) is an alternative way to direct the assembly process towards the formation of different structures (e.g., lacunary structures) and influence the electronic properties of the clusters [30–32]. Lacunary POMs can be formed by expulsion of some atoms from the complete structure, which tends to increase the nucleophilicity and consequently the reactivity of the formed clusters towards electrophiles. This provides a unique opportunity for the formation of larger architectures by reacting under appropriate experimental conditions unsaturated POM structures with transitional metals, Figure 5, lanthanides and metal complexes [25]. Finally, it is

clear that the plethora of design approaches and wide range of experimental parameters that can influence the self-assembly process allows the preparation of an immense variety of POM architectures with different sizes, compositions and properties, in a controllable fashion.

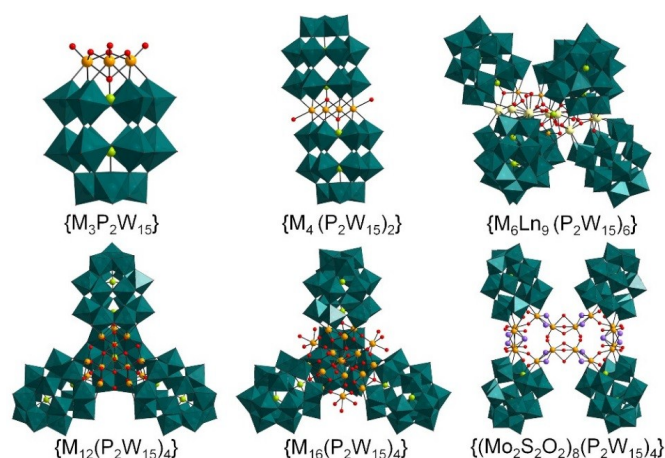


Figure 5. Representation of the transition metal substituted POM structures derived from the $\{P_2W_{15}\}$ lacunary species. From top left: $\{M_3P_2W_{15}\}$ [33–35]; $\{M_4(P_2W_{15})_2\}$ [36–39]; $\{M_6Ln_9(P_2W_{15})_6\}$ [40]; $\{M_{12}(P_2W_{15})_4\}$ [41]; $\{M_{16}(P_2W_{15})_4\}$ [42]; $\{(Mo_2O_2S_2)_8(P_2W_{15})_4\}$ [43]. (Colour scheme: W, teal; O, red; Sulfur, purple; Heteroatom, lime green; Transition metals, orange; Lanthanide, pale yellow).

Interestingly, polyoxometalate clusters have the tendency to interact constructively with other inorganic or inorganic moieties and form supramolecular aggregates. For example, since 2008 and the research of Mizuno et al. who reported the first hybrid complexes based on cucurbit[n]uril (CB[n]) and polyoxometalates [44] (Figure 6), various hybrid molecular solids based on POMs and CB[n] derivatives have been investigated. The hybrid system of POMs and CB[n] has gained great interest due to distinctive structural features. Recently, Lü and co-workers reported the first example of hybrid solids based on Lindqvist-type POM anions $[W_6O_{19}]^{2-}$ and dexamethylcucurbit[5]uril ($Me_{10}CB[5]$) [45]. In the reported compound, $\{[Na_2(W_6O_{19})(Me_{10}CB[5])(H_2O)] \cdot 2H_2O\}_n$, the sodium ions, $[W_6O_{19}]^{2-}$ anions and $Me_{10}CB[5]$ form 1D chains that are held together through supramolecular non-bonding interactions such as C–H $\cdots\pi$, dipole–dipole and hydrogen bonds resulting in a 3D supramolecular host–guest network. The compound exhibits enhanced photocatalytic property for dye degradation under visible light, due to cooperative effects induced by its components.

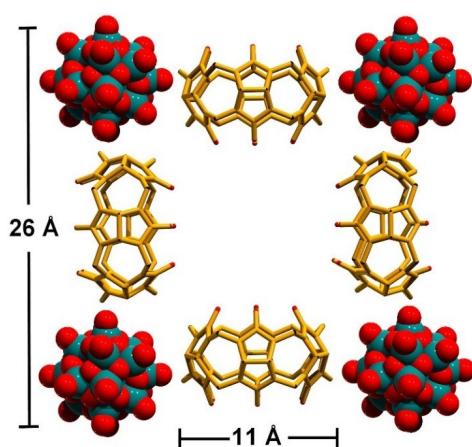


Figure 6. Representation of intermolecular interactions between the $\{V_{18}\}$ and cucurbit[n]uril molecules forming a 1D square shaped channel.

In a similar approach, cyclodextrins (CDs) are cyclic oligosaccharides comprised of 6 to 8 glucose units exhibiting torus-shaped ring structure comparable to the CB moieties discussed above. An important distinction, though, is that the interior cavity of CDs is hydrophobic, while the exterior side is hydrophilic; due to this architectural conformation, they can incorporate organic and inorganic guest molecules of appropriate size. The main driving force in this case are dipole–dipole, electrostatic forces, hydrogen bonding and van der Waals interactions [46,47]. Very recently, Cadot et al. reported the isolation of the 1:1, 1:2, 1:3 adducts, which are formed due to the attractive interactions including electrostatic, ion-dipole and hydrogen bonding between the longitudinal side of Dawson anion $[P_2W_{18}O_{62}]^{6-}$ and primary face of γ -CD, as well as a complex that is consisted of a cationic octahedral cluster $[Ta_6Br_{12}(H_2O)_6]^{2+}$ and γ -CD, which is held together by intermolecular interactions [48]. Additionally, the authors demonstrated that the interaction of three constituents ($[P_2W_{18}O_{62}]^{6-}$, $[Ta_6Br_{12}(H_2O)_6]^{2+}$, γ -CD) generate a three-component supramolecular hybrid system. In this case, the $[Ta_6@2CD]^{2+}$ unit acts as a ditopic ionic linker forming a tubular chain with periodic alternation of POMs and clusters. The same group reported a three-component hybrid assembly organized through non-covalent interactions [49]. The supramolecular aggregate is based on the nano-sized $[Mo_{154}O_{462}H_{14}(H_2O)_{70}]^{14-}$ molybdenum blue wheel, which hosts a Dawson cluster, $[P_2W_{18}O_{62}]^{6-}$ which is capped by two γ -CDs moieties. The three components are held together by intermolecular interactions (Figure 7).

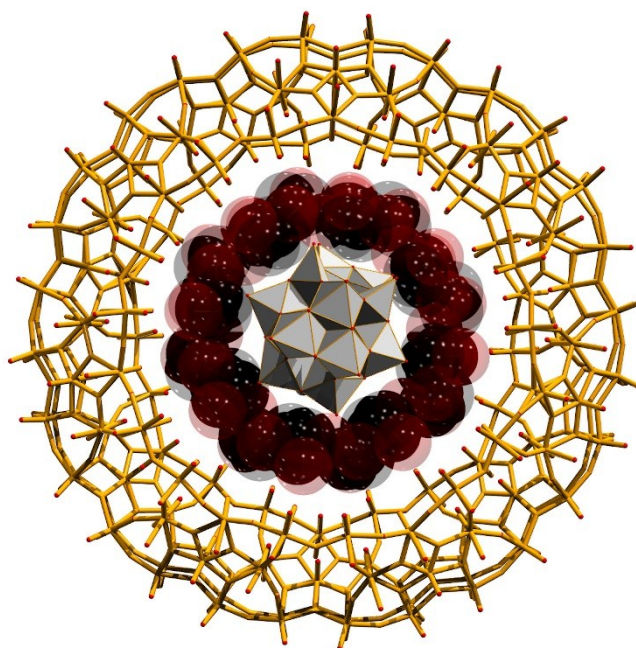


Figure 7. Representation of the $[Mo_{154}O_{462}H_{14}(H_2O)_{70}]^{14-}$ molecular wheel which hosts a Dawson anion, $[P_2W_{18}O_{62}]^{6-}$, capped by two γ -CDs moieties.

2.2. POM-OFs

Polyoxometalate open frameworks (POM-OFs) are extended architectures that can be constructed using POM-based clusters as building blocks. The interplay of supramolecular interactions (through hydrogen bonds, van der Waals forces), as well as reactivity between POM clusters and transition metals or metal complexes, can lead to the formation of extended networks of coordinatively linked 1D chains, 2D sheets and 3D compounds. As shown in the figure below, the POM clusters can be linked through transitional metals (TM) via grafted organic units, directly through transition metals, through organic linkers and through organic linkers via transition metals (Figure 8) [50]. POM-OFs are porous materials with interesting structural flexibility, stability and interesting physical properties.

Moreover, the ability of POM species to accept and release electrons reversibly with marginal structural changes makes them exceptional candidates for catalytic applications.

In 2017, Chang et al. following the above approach reported the synthesis of the networked compound $(en)[Cu_3(ptz)_4(H_2O)_4][Co_2Mo_{10}H_4O_{38}] \cdot 24H_2O$, which is the first 3D host–guest structure with an Evans-Showell type polyoxometalate as the guest (Figure 9), while the compounds $(Hbim)_2\{[Cu(bim)_2(H_2O)_2]_2[Co_2Mo_{10}H_4O_{38}]\} \cdot 5H_2O$ and $H_2[Cu(dpdo)_3(H_2O)_4][Cu_2(dpdo)_3(H_2O)_4(CH_3CN)]_2\{Co_2Mo_{10}H_4O_{38}\}_2 \cdot 9H_2O$ are the first 2D hybrid networks that include this type of POM archetype [51]. In contrast with other POM building blocks (Keggin, Dawson), the reported examples of Evans-Showell-based hybrids are quite rare. All three compounds showed promising catalytic efficiency in the oxidation of sulfides and alcohols.

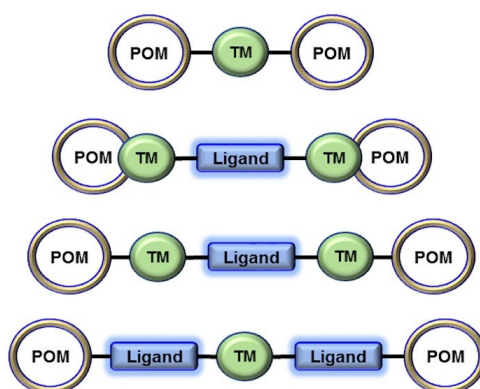


Figure 8. The four types of POM–Ligand connectivities.

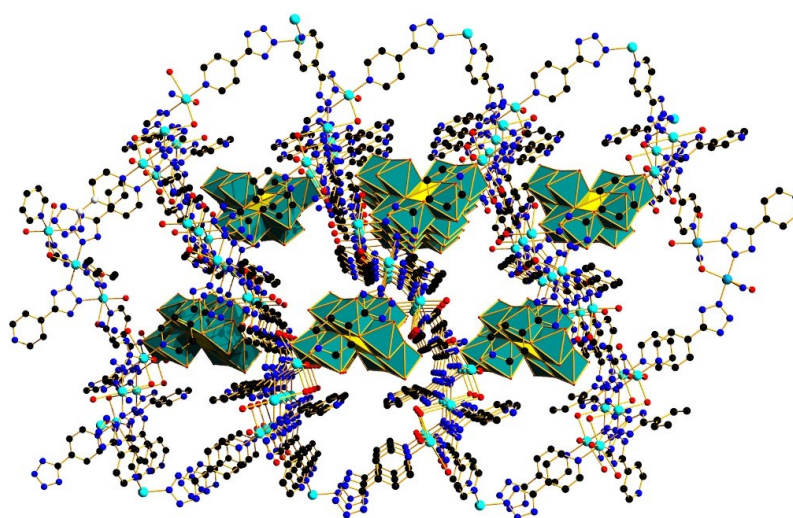


Figure 9. Representation of $(en)[Cu_3(ptz)_4(H_2O)_4][Co_2Mo_{10}H_4O_{38}]$ compound. 3D host–guest framework (ball-and-stick) with two enantiomers of $[Co_2Mo_{10}H_4O_{38}]^{6-}$ (polyhedral representation) as the guest. (Colour scheme: Mo, teal; O, red; Cu, cyan; Co, yellow; C, black; N, blue; Lanthanide, pale yellow).

In a similar manner, Liu et al. utilized [10] Anderson and octamolybdate-based clusters and Cu^{II} -based complexes to prepare a new family of hybrid networked compounds which exhibit a variety of dimensions: $[Cu_2(2-pdya)(CrMo_6(OH)_5O_{19})(H_2O)_2] \cdot 3H_2O$, $[Cu(3-dpye)_{0.5}(\gamma-Mo_8O_{26})_{0.5}(H_2O)_4] \cdot H_2O$, $[Cu(4-Hdppy)_2(\beta-Mo_8O_{26})(H_2O)_2] \cdot 4H_2O$, $[Cu_4(\mu_3-OH)_2(H_2O)_4(3-dpyh)(\gamma-Mo_8O_{27})] \cdot 4H_2O$, $[Cu_2(4-Hdpye)_2(TeMo_6O_{24})(H_2O)_6] \cdot 4H_2O$, $[Cu_3(3-dpyb)_2(TeMo_6O_{24})(H_2O)_8] \cdot 4H_2O$, $[Cu_2(4-Hdpyb)_2(TeMo_6O_{24})(H_2O)_6] \cdot 4H_2O$, (3-dpye = N,N' -bis(3-pyridinecarboxamide)-1,2-ethane, 4-dpye = N,N' -bis(4-pyridinecarboxamide)-1,2-ethane, 4-dppy = N,N' -bis(4-pyridinecarboxamide)-1,3-propane, 3-dpyb = N,N' -bis(3-

pyridinecarboxamide)-1,4-butane, 3-dpyh = *N,N'*-bis (3-pyridinecarboxamide)-1,6-hexane [52]. All compounds exhibit good electrocatalytic activities for the reduction of BrO_3^- and H_2O_2 , and photocatalytic activity towards the degradation of harmful organic dyes such as methylene blue and rhodamine B.

Another interesting example of cooperativity between supramolecular interactions and self-assembly processes is the case of the β -octamolybdate isomer, $[\beta\text{-Mo}_8\text{O}_{26}]^{4-}$. The octamolybdate cluster was used initially to coordinate through its terminal oxygen binding sites to many first row transition metal complexes. Examples include coordination to various complexes of first row transition metals (Co, Ni, Cu and Zn), allowing the formation of 2D and 3D networks [53–55]. Another prominent example of the coordination behaviour adopted by the $[\beta\text{-Mo}_8\text{O}_{26}]^{4-}$ anion is its ability to coordinate silver (I) cations using its terminal oxygen ligands enabling it to behave as a bi-, tetra-, or hexadentate ligand [56–58]. For example, work in this area by Cronin et al. revealed that reaction of the molybdenum Lindqvist anion, $[\text{Mo}_6\text{O}_{19}]^{2-}$ with silver (I) cations in a variety of coordinating solvents led to the isolation of various architectures involving, specifically the aggregation of $(\text{Ag}\{\text{Mo}_8\}\text{Ag})$ synthons [57]. The use of rigid, sterically bulky cations such as tetraphenylphosphonium ions in DMSO solvent allowed isolation of the structure $(\text{Ph}_4\text{P})_2[\text{Ag}_2\text{Mo}_8\text{O}_{26}((\text{CH}_3)_2\text{SO})_4]$, which is composed of ‘monomers’ of this $(\text{Ag}\{\text{Mo}_8\}\text{Ag})$ building-block [58]. In comparison, the use of varying chain-length alkylammonium cations, i.e., tetrapropyl-, tetrabutyl-, tetrahexyl-, and tetraheptylammonium ions in a range of solvents such as acetonitrile, DMSO and DMF, led to the isolation of a variety of architectures, ranging from chains, to grids and 2D networks. The generation of these different POM architectures was shown to be governed mainly by the steric requirements of the organic cations or coordinated solvent molecules. Another important feature of these results was the identification of the unusual $\{\text{Ag}_2\}$ dimers positioned between the $\{\text{Mo}_8\}$ cluster units, which are a result of the repeating $(\text{Ag}\{\text{Mo}_8\}\text{Ag})$ building-block units within these structures. This linking motif is uncommon in POM chemistry and is a rare example of d^{10} (i.e., filled d-shell) bridging units which are held together by significant argentophilic interactions, i.e., where the Ag-Ag distance is less than the sum of the van der Waals radii (3.44 Å). Moreover, POM-based clusters also attracted the attention of research groups whose work was focused on exploring their interactions in biological systems. The implemented approach involved the functionalization of POMs with organic ligands which exhibit biological activity. A family of organic compounds with these characteristics are biphosphonates, with general formula $\text{H}_2\text{O}_3\text{PC}(\text{OH})(\text{R})\text{PO}_3\text{H}_2$, which have been studied as anti-bacterial and anti-cancer agents [59], and various amino acids, like glycine and proline [60,61]. Initial exploration of the parameter space (pH, concentration, counterions effect, ionic strength, etc.) yielded a large variety of compounds with different properties which can interact with biological systems [62–67].

Utilization of a similar approach focused a lot of research efforts on exploiting the constructive interactions of the POM-OFs constituents in an effort to introduce specific functionality to the final material. For example, a lot of investigations have been dedicated into the reduction of gas emission, as well as, development of materials for water purification. Very recently, Ma et al. reported the synthesis of a 2D compound $[\text{Co}_2\text{L}_{0.5}\text{V}_4\text{O}_{12}] \cdot 3\text{DMF} \cdot 5\text{H}_2\text{O}$ (L = wheel-like resorcin[4]arene ligand), which was used as heterogeneous catalyst and exhibited high efficiency for the cycloaddition of CO_2 with epoxides and for oxidative desulfurization of sulfides [68]. It was shown that the compound’s catalytic efficiency originates from the exposed vanadium sites residing in the channels. Also, in 2016 Yang et al. synthesized a family of three compounds $[\text{PMo}_{12}\text{O}_{40}]@[\text{Cu}_6\text{O}(\text{TZI})_3(\text{H}_2\text{O})_9]_4 \cdot \text{OH} \cdot 31\text{H}_2\text{O}$ (H_3TZI = 5-tetrazolyisophthalic acid), $[\text{SiMo}_{12}\text{O}_{40}]@[\text{Cu}_6\text{O}(\text{TZI})_3(\text{H}_2\text{O})_9]_4 \cdot 32\text{H}_2\text{O}$, and $[\text{PW}_{12}\text{O}_{40}]@[\text{Cu}_6\text{O}(\text{TZI})_3(\text{H}_2\text{O})_6]_4 \cdot \text{OH} \cdot 31\text{H}_2\text{O}$ under “one-pot” solvothermal conditions, which involved the immobilization of Keggin clusters within the cavities of the rht-MOF-1 [69]. The cooperative effects due to the co-existence of MOF and POM structures proved to be beneficial for the adsorption of organic pollutants and their subsequent oxidation to useful products.

Keggin-based species have been proven to be very useful building blocks for the construction of POM-OF compounds. For example Dolbecq et al. [70] reported the preparation of four 1D

and 2D networks. More specifically, $(\text{TBA})_3\{\text{PMo}^{\text{V}}_8\text{Mo}^{\text{VI}}_4\text{O}_{36}(\text{OH})_4\text{Zn}_4\}[\text{C}_6\text{H}_4(\text{COO})_2]_2$ is a 2D compound which incorporates Zn-capped Keggin units connected via 1,3 benzenedicarboxylate (isop) linkers and tetrabutylammonium (TBA) counter-cations occupying the space between the planes. In the case of $(\text{TPA})_3\{\text{PMo}^{\text{V}}_8\text{Mo}^{\text{VI}}_4\text{O}_{37}(\text{OH})_3\text{Zn}_4\}[\text{C}_6\text{H}_3(\text{COO})_3](\text{TPA}[\text{e}(\text{trim})]_\infty)$, the Zn-capped Keggin units form 1D inorganic chains which are linked further via 1,3,5-benzenetricarboxylate (trim) ligands into an overall 2D architecture. Alternatively, in $(\text{TBA})\{\text{PMo}^{\text{V}}_8\text{Mo}^{\text{VI}}_4\text{O}_{40}\text{Zn}_4\}(\text{C}_7\text{H}_4\text{N}_2)_2(\text{C}_7\text{H}_5\text{N}_2)_2 \cdot 12\text{H}_2\text{O}(\text{e}(\text{bim})_4)$ compound the Zn capped Keggin units are connected to benzimidazole (bim) ligands. Finally, the $(\text{TBA})(\text{C}_{10}\text{H}_{10}\text{N}_4)_2(\text{HPO}_3)\text{PMo}^{\text{V}}_8\text{Mo}^{\text{VI}}_4\text{O}_{40}\text{Zn}_4\}_2(\text{C}_{10}\text{H}_9\text{N}_4)_3(\text{C}_{10}\text{H}_8\text{N}_4)(\text{e}_2(\text{pazo})_4)$ incorporates dimeric Zn capped Keggin units bridged by $[\text{HPO}_3]^{2-}$ anions and para-azobipyridine (pazo) ligands completing the coordination sphere. The group also showed the use of these compounds as environmentally friendly reducing agents for the reduction of graphite oxide (GO) to graphene (G) under mild conditions. The obtained materials' (POM@G) large surface area and noteworthy stability under various experimental conditions made them promising candidates for numerous applications such as photo/electro catalysis, electrode materials and sensors.

Another set of representative examples are the all-inorganic POM-OF compounds reported by Cronin et al. [71] where the connectivity between the POM-based building blocks was served exclusively by transition metals. The Mn-linked cubic framework, $\text{K}_{18}\text{Li}_6[\text{Mn}_8(\text{H}_2\text{O})_{48}\text{P}_8\text{W}_{48}\text{O}_{184}] \cdot 108\text{H}_2\text{O}$, incorporates 8-connected $\{\text{P}_8\text{W}_{48}\}$ units, bridged by Mn^{II} centres, located to the external surfaces of the rings (Figure 10). The cubic sub-units formed by the perpendicular orientation of the $\{\text{P}_8\text{W}_{48}\}$ rings define an infinite array nano-sized molecular cubes, enclosing roughly spherical cavities of ca. 7.2 nm^3 . The authors demonstrated the accessibility of these cavities by divalent transition metals. In a similar manner, the same group reported shortly after a whole family of POM-OFs based on the connectivity of $\{\text{P}_8\text{W}_{48}\}$ building blocks with other transitional metals (e.g., Co^{2+}). The authors showed that the conformational flexibility of the crystalline framework, which can undergo eight different crystal-to-crystal transformations without compromising either its structural stability or its crystallinity. Finally, it was shown that observed adsorption properties are directly associated with the conformational flexibility of the material.

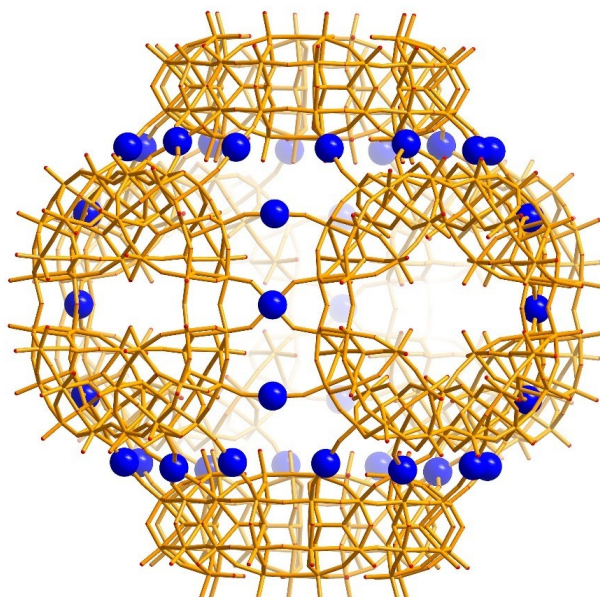


Figure 10. Representation of Mn-linked cubic framework, $\text{K}_{18}\text{Li}_6[\text{Mn}_8(\text{H}_2\text{O})_{48}\text{P}_8\text{W}_{48}\text{O}_{184}] \cdot 108\text{H}_2\text{O}$. The $\{\text{P}_8\text{W}_{48}\}$ units are connected through Mn^{II} centres to form a face-directed cube, with internal cavity volume of ca. 7.2 nm^3 . The repeated cubic units form an infinite 3D lattice. (Colour scheme: $\{\text{P}_8\text{W}_{48}\}$, orange wired representation; Mn^{II} , blue spheres).

Another sub-category of the hybrid POM-MOF-based materials is the polyoxometalate-lanthanide organic frameworks (POM-LOF), which have attracted the interest of various research groups due to their modular optical (e.g., luminescence) and magnetic properties originating from the interactions with 4f electrons of Ln^{III} cations. Very recently, the compound $[\text{Ce}_4(\text{BINDI})_2(\text{DMA})_{16}]\cdot[\text{SiW}_{12}\text{O}_{40}]\cdot 3\text{DMA}$ (BINDI = *N,N'*-bis(5-isophthalate)-1,4,5,8-naphthalenediimide, DMA = *N,N*-dimethylacetamide) was reported, which is the first example of a visible-light-responsive photochromic POM-LOF hybrid material. This compound exhibits unusual four-fold interpenetration of 3D cationic frameworks that further encapsulate non-coordinating Keggin $[\text{SiW}_{12}\text{O}_{40}]^{4-}$ species (Figure 11) [72]. The interactions between the π -acidic naphthalenediimide moieties and the anionic POM clusters played a key role in the self-organization of the components, which led to the formation of the final product.

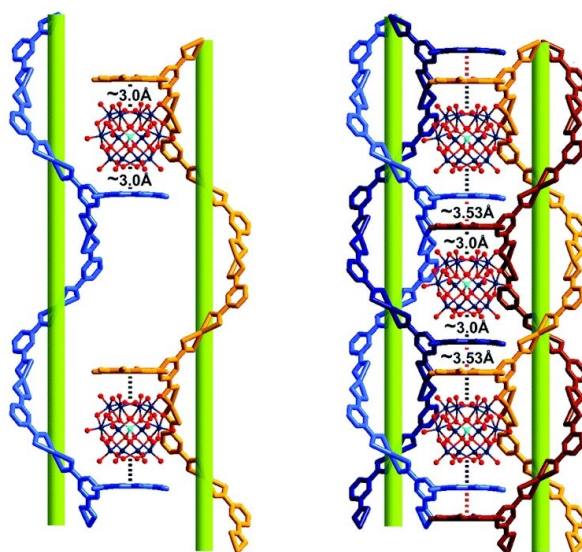


Figure 11. Keggin anions $[\text{SiW}_{12}\text{O}_{40}]^{4-}$ immobilized via anion- π interactions developed between POMs and NDIs (**left**). Structural analysis revealed two kinds of double-stranded helical chains with opposite handedness surrounded by NDI-NDI-POM-NDI-NDI sandwich arrays (**right**). Adapted from *Dalton Trans.* 2017, 46, 4898–4901. Copyright (2017) Royal Society of Chemistry.

3. Metal–Organic Coordination Frameworks

The family of porous solids is another category of self-assembled materials which exhibit interesting properties and wide range of applications. Their functionality is based mainly on their chemical and physical properties, such as porosity, surface area and thermal stability. A sub-category of solid materials, which developed dramatically during the last decades, is the metal–organic frameworks (MOFs). MOFs are porous crystalline materials, which are constructed by metal ion centres or clusters and organic linkers through coordination bonding. The term “metal–organic framework” was introduced for the first time in 1995 from Yaghi [73]. The structure and the properties of MOFs depends on the choice of metal centres, as well as the metal’s coordination number, which consequently influences the shape and the pore size. Also, the organic ligands play an equally important role due to their chemical reactivity, physical properties, geometry, and the non-covalent interactions that can develop [74,75].

The implementation of some design approaches can lead to construction of functionalized structures with a wide range of applications. The two common methods utilized for the functionalization of MOFs are the pre-synthetic modification, where the components are pre-functionalized and form the desired MOF-based architecture, and the post-synthetic modification, where the modification takes place after the preparation of the MOF-based progenitor. An example of pre-synthetic modification is the synthesis of the rht-type MOF structure, $[\text{Co}_{24}(\text{TPBTM})_8(\text{H}_2\text{O})_{24}]$,

where the TPBTM is an amide functionalized trigonal carboxylate linker [76]. This compound exhibited greater affinity for CO₂ molecules in comparison with the compound [Co₂₄(bte)₈(H₂O)₂₄], due to dipole-quadrupole interactions and hydrogen bonds developed between the acylamide groups and the CO₂ molecules. On the other hand, Kitagawa et al. reported an elegant example of post-synthetic modification via coordinative surface ligand exchange [57] of two Zn-based MOFs: [Zn₂(1,4-bdc)₂(dabco)]_n and [Zn₂(1,4-ndc)₂(dabco)]_n (Figure 12) [77].

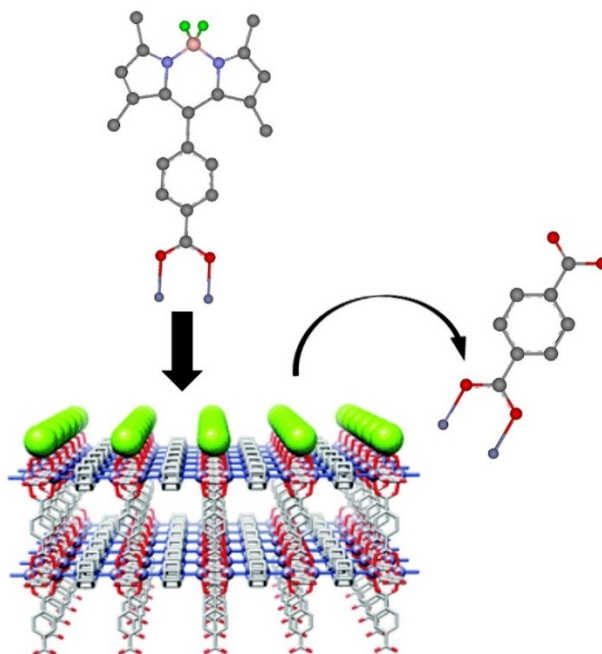


Figure 12. Exchange of surface ligands, 1,4-benzenedicarboxylate units (1,4-bdc) by the fluorescent boron dipyrromethene linkers. (Colour scheme: Zn, purple; O, red; B, pink; Co, yellow; C, dark grey; N, blue; F, green).

MOF materials can be synthesized with various methods, and each one offers its own advantages. The synthetic procedures typically involve the following: (a) solvothermal synthesis: the most commonly used method, in which the reagents are heated in solution in closed vessels under autogenous pressure; (b) slow evaporation method: this does not need a supply of additional energy, but requires more time than other techniques, and is rarely used due to solubility issues; (c) electrochemical synthesis: the synthesis is carried out under mild reaction conditions, where real-time control/modification of the reaction parameters is possible; (d) mechanochemical synthesis: a solvent-free, economical chemical reaction driven by mechanical force; (e) microwave-assisted synthesis: rapid method for MOF synthesis, and it has been used to produce nanosized metal oxides; and (f) sonochemical synthesis: implementation of intensive ultrasonic radiation that triggers chemical and physical changes, which leads to the reduction of crystallization times. As a new class of porous solid materials, MOFs are attractive candidates for a variety of industrial applications due to their physical and chemical properties such as high porosity, high surface area, and modular surface. Some representative applications are summarized below:

3.1. Catalysis and Gas Storage

Catalysis is one of the most studied area of applications for MOF-based materials [78–80]. The porous nature of MOF structures allows the efficient diffusion of the substrates towards the catalytic sites (Figure 13). Taking into consideration the fact that the catalytic sites, as well as the interactions within the pores, can be tuned by employing rational structure design approaches, these are ideal

candidates for catalytic applications. The compound MIL-101(Cr) is used in catalytic reactions due to the presence of free Lewis acid sites when water molecules are removed (Figure 14). Another important application field for MOF-based materials is the storage of small gas molecules [81–83]. Also, in this case, utilizing design principles is crucial for tailoring the structure for specific application such as engineering of the pores' size and the chemical environment within the pores in order to optimize the affinity of the material towards specific substrates [84].

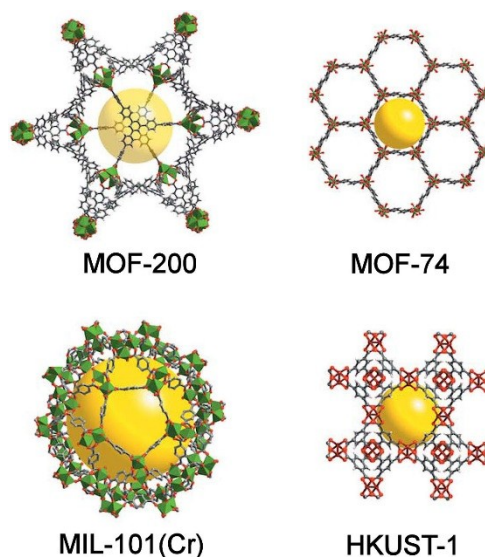


Figure 13. Representative types of MOF structures which exhibit high gas storage properties. MOF-200: H₂; MOF-74: CO₂, NO, CH₄; MIL-101(Cr): H₂, CO₂; HKUST-1: CO₂, NO, CH₄.

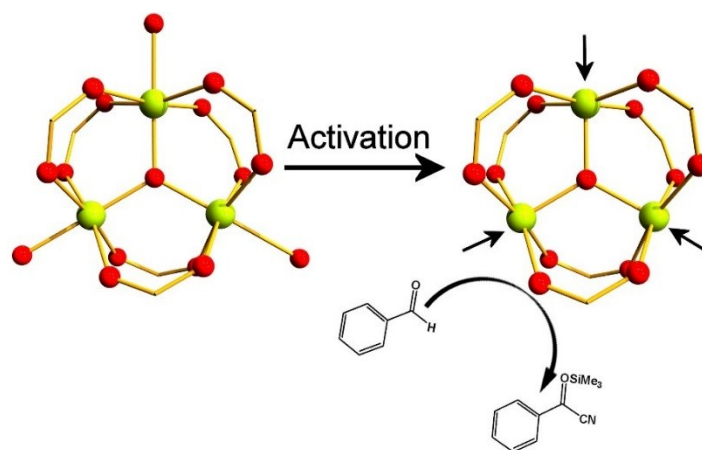


Figure 14. The coordinated water molecules are removed from MIL-101(Cr) generating free coordination sites (highlighted with black arrows) during the activation process. Subsequently, the activated MIL-101(Cr) catalyses the cyanosilylation of benzaldehyde. (Colour scheme: Fe, lime green; O, red).

3.2. Drug Delivery Systems (DDS)

The last decade, in an effort to exploit the inherent properties of MOFs, such as porosity, modular surface chemistry, large surface areas, and tunable pore sizes, various research groups explored the potential uses of MOF-based materials as drug delivery systems [85,86]. The low chemical and aqueous stability of some MOF structures render them highly promising candidates for drug delivery applications, taking into consideration that MOF structural units need to be biodegraded after the drug release.

Very recently, Forgan et al. reported the synthesis and characterization of a Zr-based family of MOFs. This family of MOFs are made of biocompatible components which can penetrate the cells' boundaries, and therefore can be used as potential materials for DDS. In this case, The MOF structures have been loaded with fluorescent molecules (e.g., calcein), and demonstrated the use of mechanical amorphisation processes for the controlled delivery of the guest molecules (Figure 15). The research results showed that the fine balance between the material's pores and the guest molecules is crucial for achieving effective release of the guest molecules [87].

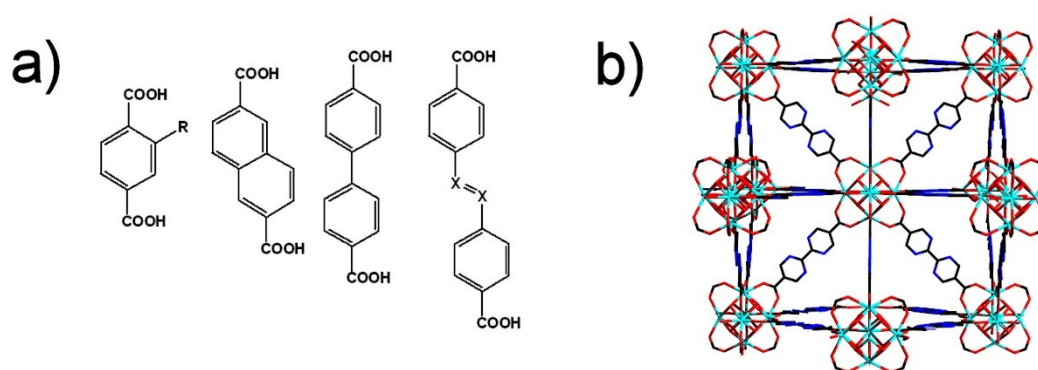


Figure 15. Structure of the organic linkers used in the MOF synthesis (a), and the structure of Zr-L₆ MOF (b). (Colour scheme: Zn, cyan; O, red; C, black; N, blue).

4. Supramolecular Interactions in LDH Materials

Layered double hydroxides (LDHs) are a class of two-dimensional clays, consisting of positively charged brucite-like layers and interlayer compensating anions. Their composition is described by the general formula $[M^{II}_{1-x}M^{III}_x(OH)_2]^{x+}[A^{m-}_{x/m}] \cdot nH_2O$ (Figure 16), where M^{II} , M^{III} are divalent (e.g., Mn, Zn) and trivalent (e.g., Al, Fe) metal ions, while A^{m-} represents interlayer anions (e.g., SO_4^{2-} , CO_3^{2-}). The formation of LDH-based materials is driven by weak interlayer interactions, and as a consequence, they offer an excellent opportunity for the development of composite compounds by exchanging the anionic and solvent content of the interlayer cavities with the desirable components. For example, exploitation of supramolecular interactions between the LDH layers and POM clusters, have given a wide range of materials with interesting catalytic properties tailored for applications in epoxidations, N-oxidations and desulfurisations [88–92].

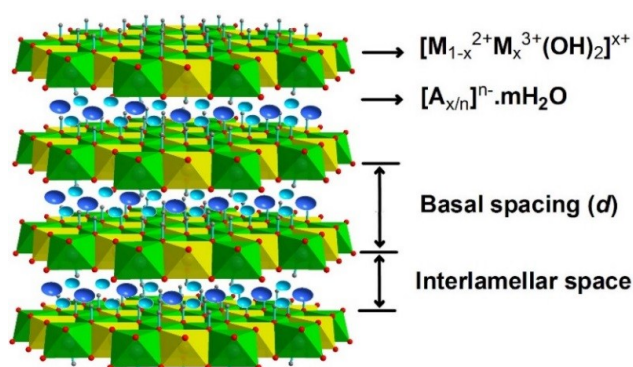


Figure 16. Schematic representation of the classical LDHs structure [88]. Adapted from Catalysts 2017, 7, 260.

As described earlier, MOFs are ideal candidates for the development of membrane materials for gas separation, due to their pore size flexibility, and their sorption properties [93,94]. However, the limited progress observed in the field of MOF-based membranes is mainly due to the weak

interfacial bonding between MOF-based membranes and chemical inert substrates, such as α - Al_2O_3 . An efficient means employed for the immobilization of MOF clusters on substrates, is the use of an LDH network. Recently, a novel seeding method for the preparation of ZIF-8 membrane on the porous substrate α - Al_2O_3 , was reported [95]. The research group demonstrated the self-organization of a network made of crystallographically vertically aligned LDH walls, which prevented the detachment of ZIF-8 seeds. The prepared ZIF-8 membrane exhibited H_2 permeance and high H_2 selectivity.

Moreover, Han et al. reported the construction of LDH@ZIF-8 composite, by in situ growth of ZIF-8 on Zn–Al–LDH, without adding any zinc precursor (Figure 17). The resulting material exhibits CO_2 adsorption capacity of $1 \text{ mmol} \cdot \text{g}^{-1}$ at room temperature and 1 bar, which is higher than Zn–Al–LDH or ZIF-8 [96] and is the result of cooperative effects developed between the LDH and ZIF-8 components of the assembled material.

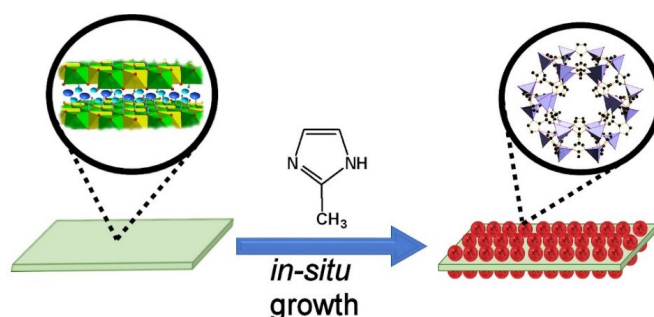


Figure 17. In situ growth of ZIF-8 nanocrystals on Zn–Al–LDH. (Colour scheme: Zn, purple; C, black; H_2O , blue spheres; A^{n-} , cyan spheres). Adapted from *Dalton Trans.* **2016**, *45*, 12632–12635. Copyright (2016) Royal Society of Chemistry.

5. Transition Metal Coordination Cages

Supramolecular coordination complexes (CCS) are finite supramolecular compounds formed by the self-assembly of metal centres in the presence of various ligands with appropriate binding sites and geometrical features. The formation of this family of compounds is driven by self-assembly processes, during which the thermodynamically favoured product is synthesized. The constituents of various coordination abilities and geometries that co-exist in the reaction mixture have the tendency to undergo a self-sorting process via a network of dynamic equilibria which appears to “correct” mis-alignments of building blocks or non-efficient types of coordination, ultimately promoting the formation of the most stable species in solution. In 1990, Fujita et al. reported the rational synthesis of a tetragonal metal complex, which consists of four linear ligands (4,4'-bipyridine) held together by four [enPd(II)] units (Figure 18) [97]. The palladium-based building block exhibits a 90° coordination angle, which ultimately drives the formation of the specific compound. Thus, the structural features and coordination angles of the components present in the reaction mixture are crucial for directing the assembly process towards the formation of a wide range of compounds, such as cages and capsules [98].

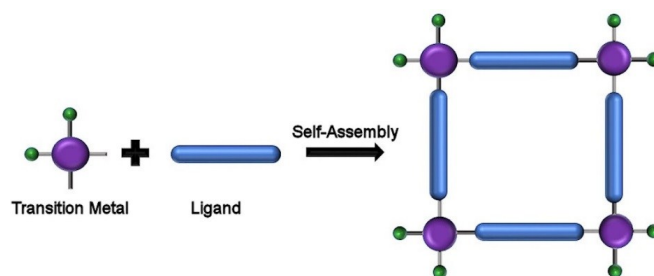


Figure 18. Representation of the tetragonal metal complex construction.

Both the metal's coordination angle and the ligand's binding site angle play a key role in the formation of new structures with different geometries. Shortly after, the same group reported the synthesis of a $M_{24}L_{48}$ rhombicuboctahedron, by simply controlling the angle between the binding sites of the dipyriddy donor ligand [99]. The use of ditopic building blocks led to the formation of 2D convex polygons, while the combination of ditopic and tritopic building blocks led to the formation of 3D polygons (Figures 19 and 20) [100]. Also, the presence of capping ligands is very important for the implementation of design elements and synthesis of diverse compounds, since they prevent the formation of infinite arrays and 1D coordination chains, while they introduce the desirable directionality.

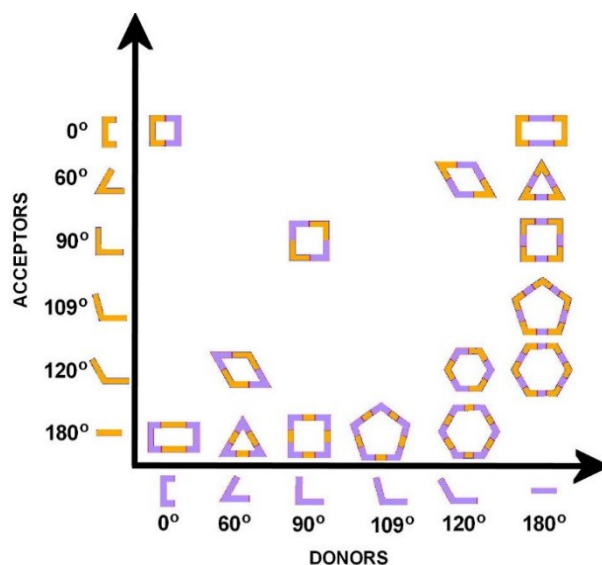


Figure 19. Formation of 2D architectures constructed by self-assembly of ditopic building blocks. Adapted from *Chem. Rev.* 2011, 111, 6810–6918. Copyright (2011) Royal Society of Chemistry.

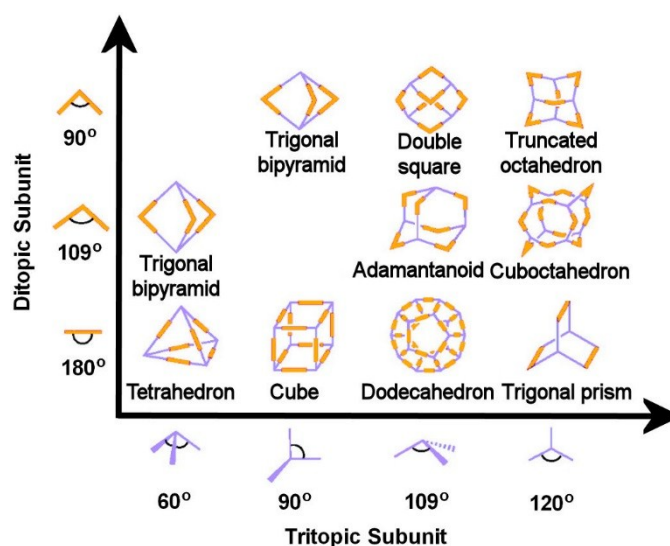


Figure 20. Formation of 3D architectures constructed by self-assembly of ditopic and tritopic building blocks. Adapted from *Chem. Rev.* 2011, 111, 6810–6918. Copyright (2011) Royal Society of Chemistry.

Supramolecular coordination complexes have attracted the attention of various research [101,102] groups due to their applications in catalysis [103], recognition and separation [104], stabilization of sensitive species [105], etc. The ability of incorporating different functional groups to coordination

cages during the self-assembly process renders the final compounds excellent candidates for rational design of supramolecular nanoreactors [106]. Very often, the guest molecules are encapsulated centrally due to their solvophobicity and size complementarity between guests and hosts. Occasionally, the nanocages are able to accommodate more than one guest depending on their size of the host cage and the guest molecule. Nitschke et al. reported the synthesis of a new class of supramolecular $M^{II}_6L_4$ pseudo-octahedra which can interact with guest molecules both internally and externally [107]. Moreover, the group demonstrated the importance of peripheral guests which template the formation of the $Cu^{II}_6L_4$ structure; they showed that the cage would be able to form based only on the self-assembly process or central template considerations.

The environment inside the cavity is very different from the bulk solution, and this is the main reason that the encapsulated molecules demonstrate different chemical behaviour. Under appropriate conditions, unique reactions can be carried out within the cage which are not generally favoured in the reaction medium; this is extremely important in several applications, including catalysis [108]. Fujita et al. investigated the encapsulation of dinuclear compounds which exhibit weak metal–metal bonds utilizing a cage-type nanoreactor (Figure 21). In this case, the ruthenium complex, $[(\eta\text{-}5\text{-indenyl})Ru(CO)_2]_2$, adopts a CO-bridged *cis* configuration and an unexpected enhancement of its photostability is observed [109]. Furthermore, the confined space of the nanocage prevents the dissociation of the metal–metal bond, which is generally favoured out of the cage. It has been reported that the compound $[(Me_4Cp)Ru(CO)_2]_2$ (Cp = cyclopentadienyl) undergoes photosubstitution of a CO ligand by an alkyne without dissociation of the Ru–Ru bond, and a Ru–alkyne π -complex is formed [110].

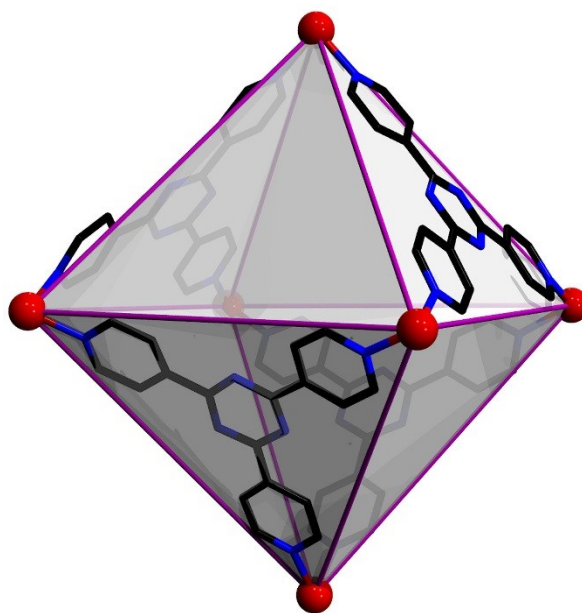


Figure 21. Representation of the $M^{II}_6L_4$ type cage reported by Fujita et al. Colour code: Pd, red spheres; C, black; N, blue.

The solubility and host/guest capabilities of supramolecular coordination systems renders them highly promising candidates for biomedical applications. Stang et al. synthesised eight tetranuclear rectangles employing a coordination self-assembly approach between arene–Ru-based acceptors and 3-bipyridyl donors. Interestingly, the research group investigated the *in vitro* cytotoxicities relative to *cis*-platin and doxorubicin. Four of these compounds exhibited notable activity (Figure 22) [111].

Finally, the CCSs nano-structures can also be used as selective molecular sensors. Chi and co-workers reported the synthesis of two heterometallic self-assembled molecular squares and studied their potential functionality as sensors for the selective detection of picric acid [112] (Figure 23).

It is worth noting at this point that the examples we discussed above do not constitute an exhaustive list of available families of clusters. There are numerous other interesting metal coordination cages with remarkable structural features and properties [113–117]. Any effort to discuss every available family of clusters, their general features and functionality would have been fruitless and goes beyond the scope of the present article.

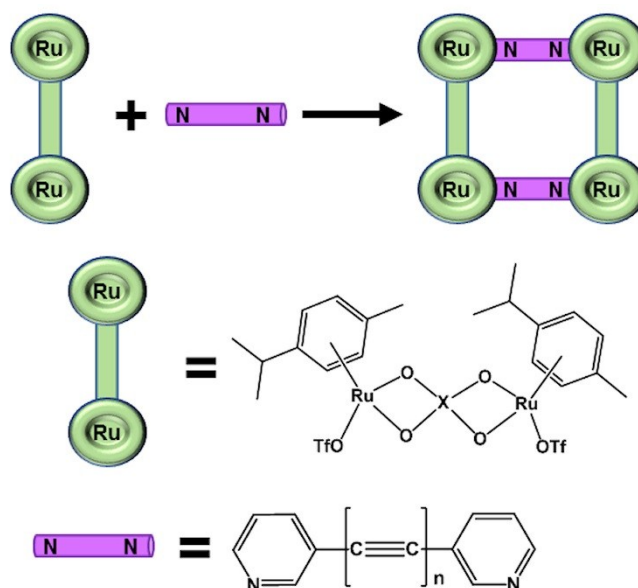


Figure 22. Self-assembly of tetranuclear molecular rectangles.

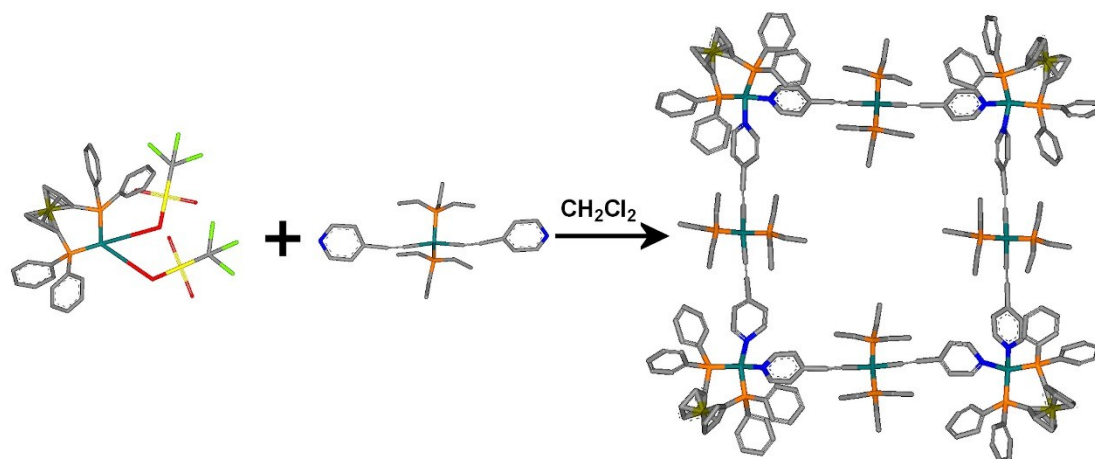


Figure 23. Heterometallic self-assembled square-shaped molecular sensor. (Colour scheme: Pd/Pt, teal; Fe, dark yellow; C, grey; N, blue; O, red; S, yellow; P, orange; F, bright green). Adapted from *Chem. Rev.* 2012, 41, 3046–3052. Copyright (2011) Royal Society of Chemistry.

6. Conclusions

In summary, supramolecular non-covalent interactions and molecular self-assembly has proven to be powerful tools in synthetic chemistry, which have been employed for the construction of compounds made by primary and secondary (cluster-based) building blocks. Both processes are driven by specific physical or chemical parameters, such as recognition processes, templating effects and chemical reactivity. Efforts to understand and ultimately control such dynamic behaviour are challenging, but also exciting, since the embedded error correction mechanism offered by the reversibility of the metal–ligand bonding, in combination with the geometrically defined metal coordination environment,

renders the self-assembly processes a particularly fruitful approach for the construction of complex structures. Incremental understanding and control over the covalent and non-covalent interactions, and their subsequent utilization as synthetic tools in chemical systems, led to the development of new families of compounds with impressive functionalities. As discussed above, polyoxometalate, metal organic frameworks and supramolecular coordination compounds are all families of compounds with unique physical and chemical properties whose formation is based on the cooperative effect of self-assembly and supramolecular interactions. The implementation of design principles using appropriate building blocks led to the emergence of functionalities based on cooperative effects developed between the self-assembled constituents. The properties that these materials exhibit range from gas storage, drug delivery, selective sensors and membranes to catalysis, stabilization of short-lived species and chemical conversions to useful products. Moreover, the coupling of these processes between the solution and solid-state offers a unique opportunity for the future development of materials with desirable functionality. We are confident that the observed exponential growth of well-defined architectures in the area of self-assembled inorganic and metal–organic systems in combination of the deeper understanding of the underlying processes, will be followed by an explosion in functionalities; taking advantage of design principles for the construction of building blocks with appropriate geometry, physical and chemical behaviour, will allow us to engineer highly sophisticated chemical systems with unprecedented properties.

Author Contributions: The paper was written jointly with equal contributions from S.P., T.A.K., Y.-F.S. and H.N.M.

Funding: This research received no external funding.

Acknowledgments: This work has been supported by The University of Glasgow.

Conflicts of Interest: The authors declare no conflict of interest.

References

1. Lehn, J.-M. Supramolecular Chemistry—Scope and Perspectives Molecules, Supermolecules, and Molecular Devices (Nobel Lecture). *Angew. Chem. Int. Ed. Engl.* **1988**, *27*, 89–112. [[CrossRef](#)]
2. Lehn, J.-M. From supramolecular chemistry towards constitutional dynamic chemistry and adaptive chemistry. *Chem. Soc. Rev.* **2007**, *36*, 151–160. [[CrossRef](#)] [[PubMed](#)]
3. Lehn, J.-M. Toward complex matter: Supramolecular chemistry and self-organization. *Proc. Natl. Acad. Sci. USA* **2002**, *99*, 4763–4768. [[CrossRef](#)] [[PubMed](#)]
4. Liu, T.; Diemann, E.; Li, H.; Dress, A.W.M.; Müller, A. Self-assembly in aqueous solution of wheel-shaped Mo₁₅₄ oxide clusters into vesicles. *Nature* **2003**, *426*, 59–62. [[CrossRef](#)] [[PubMed](#)]
5. Liu, T.; Imber, B.; Diemann, E.; Liu, G.; Cokleski, K.; Li, H.; Chen, Z.; Müller, A. Deprotonations and Charges of Well-Defined {Mo₇₂Fe₃₀} Nanoacids Simply Stepwise Tuned by pH Allow Control/Variation of Related Self-Assembly Processes. *J. Am. Chem. Soc.* **2006**, *128*, 15914–15920. [[CrossRef](#)] [[PubMed](#)]
6. Wilson, E.F.; Miras, H.N.; Rosnes, M.H.; Cronin, L. Real-time observation of the self-assembly of hybrid polyoxometalates using mass spectrometry. *Angew. Chem. Int. Ed.* **2011**, *50*, 3720–3724. [[CrossRef](#)] [[PubMed](#)]
7. Miras, H.N.; Wilson, E.F.; Cronin, L. Unravelling the complexities of inorganic and supramolecular self-assembly in solution with electrospray and cryospray mass spectrometry. *Chem. Commun.* **2009**, 1297–1311. [[CrossRef](#)] [[PubMed](#)]
8. Miras, H.N.; Richmond, C.J.; Long, D.L.; Cronin, L. Solution-phase monitoring of the structural evolution of a Molybdenum Blue nanoring. *J. Am. Chem. Soc.* **2012**, *134*, 3816–3824. [[CrossRef](#)] [[PubMed](#)]
9. Yoneya, M.; Yamaguchi, T.; Sato, S.; Fujita, M. Simulation of Metal–Ligand Self-Assembly into Spherical Complex M₆L₈. *J. Am. Chem. Soc.* **2012**, *134*, 14401–14407. [[CrossRef](#)] [[PubMed](#)]
10. Yoneya, M.; Tsuzuki, S.; Yamaguchi, T.; Sato, S.; Fujita, M. Coordination-Directed Self-Assembly of M₁₂L₂₄ Nanocage: Effects of Kinetic Trapping on the Assembly Process. *ACS Nano* **2014**, *8*, 1290–1296. [[CrossRef](#)] [[PubMed](#)]
11. Miras, H.N.; Cooper, G.J.T.; Long, D.-L.; Bögge, H.; Müller, A.; Streb, C.; Cronin, L. Unveiling the transient template in the self-assembly of a molecular oxide nanowheel. *Science* **2010**, *327*, 72–74. [[CrossRef](#)] [[PubMed](#)]

12. Hou, Y.; Zakharov, L.N.; Nyman, M. Observing Assembly of Complex Inorganic Materials from Polyoxometalate Building Blocks. *J. Am. Chem. Soc.* **2013**, *135*, 16651–16657. [[CrossRef](#)] [[PubMed](#)]
13. Nyman, M. Polyoxoniobate chemistry in the 21st century. *Dalton Trans.* **2011**, *40*, 8049. [[CrossRef](#)] [[PubMed](#)]
14. Nelson, W.H.; Tobias, R.S. Structure of the Polyanions of the Transition Metals in Aqueous Solution: The Hexatantalate. *Inorg. Chem.* **1963**, *2*, 985–992. [[CrossRef](#)]
15. Li, S.; Liu, S.; Liu, S.; Liu, Y.; Tang, Q.; Shi, Z.; Ouyang, S.; Ye, J. $\{Ta_{12}\}/\{Ta_{16}\}$ Cluster-Containing Polytantalotungstates with Remarkable Photocatalytic H_2 Evolution Activity. *J. Am. Chem. Soc.* **2012**, *134*, 19716–19721. [[CrossRef](#)] [[PubMed](#)]
16. Xiang, Y.; Izarova, N.V.; Schinle, F.; Hampe, O.; Keita, B.; Kortz, U. The selenite-capped polyoxo-4-aurate(III), $[Au^{III}_4O_4(Se^{IV}O_3)_4]^{4-}$. *Chem. Commun.* **2012**, *48*, 9849. [[CrossRef](#)] [[PubMed](#)]
17. Izarova, N.V.; Vankova, N.; Heine, T.; Biboum, R.N.; Keita, B.; Nadjo, L.; Kortz, U. Polyoxometalates Made of Gold: The Polyoxoaurate $[Au^{III}_4As^V_4O_{20}]^{8-}$. *Angew. Chem. Int. Ed.* **2010**, *49*, 1886–1889. [[CrossRef](#)] [[PubMed](#)]
18. Barsukova, M.; Izarova, N.V.; Biboum, R.N.; Keita, B.; Nadjo, L.; Ramachandran, V.; Dalal, N.S.; Antonova, N.S.; Carbó, J.J.; Poblet, J.M.; et al. Polyoxopalladates Encapsulating Yttrium and Lanthanide Ions, $[X^{III}Pd^{II}_{12}(AsPh)_8O_{32}]^{5-}$ ($X = Y, Pr, Nd, Sm, Eu, Gd, Tb, Dy, Ho, Er, Tm, Yb, Lu$). *Chem. A Eur. J.* **2010**, *16*, 9076–9085. [[CrossRef](#)] [[PubMed](#)]
19. Yang, P.; Xiang, Y.; Lin, Z.; Lang, Z.; Jiménez-Lozano, P.; Carbó, J.J.; Poblet, J.M.; Fan, L.; Hu, C.; Kortz, U. Discrete Silver(I)-Palladium(II)-Oxo Nanoclusters, $\{Ag_4Pd_{13}\}$ and $\{Ag_5Pd_{15}\}$, and the Role of Metal–Metal Bonding Induced by Cation Confinement. *Angew. Chem. Int. Ed.* **2016**, *55*, 15766–15770. [[CrossRef](#)] [[PubMed](#)]
20. Yang, P.; Li, H.; Ma, T.; Haso, F.; Liu, T.; Fan, L.; Lin, Z.; Hu, C.; Kortz, U. Rational Design of Organically Functionalized Polyoxopalladates and Their Supramolecular Properties. *Chem. A Eur. J.* **2018**, *24*, 2466–2473. [[CrossRef](#)] [[PubMed](#)]
21. Chubarova, E.V.; Dickman, M.H.; Keita, B.; Nadjo, L.; Miserque, F.; Mifsud, M.; Arends, I.W.C.E.; Kortz, U. Self-Assembly of a Heteropolyoxopalladate Nanocube: $[Pd^{II}_{13}As^V_8O_{34}(OH)_6]^{8-}$. *Angew. Chem. Int. Ed.* **2008**, *47*, 9542–9546. [[CrossRef](#)] [[PubMed](#)]
22. Izarova, N.V.; Pope, M.T.; Kortz, U. Noble Metals in Polyoxometalates. *Angew. Chem. Int. Ed.* **2012**, *51*, 9492–9510. [[CrossRef](#)] [[PubMed](#)]
23. Vilà-Nadal, L.; Cronin, L. Design and synthesis of polyoxometalate-framework materials from cluster precursors. *Nat. Rev. Mater.* **2017**, *2*, 17054. [[CrossRef](#)]
24. Miras, H.N.; Long, D.-L.; Cronin, L. Exploring Self-Assembly and the Self-Organization of Nanoscale Inorganic Polyoxometalate Clusters. In *Polyoxometalate Chemistry*; Elsevier Inc.: Cambridge, MA, USA, 2017; Volume 69.
25. Long, D.L.; Tsunashima, R.; Cronin, L. Polyoxometalates: Building blocks for functional nanoscale systems. *Angew. Chem. Int. Ed.* **2010**, *49*, 1736–1758. [[CrossRef](#)] [[PubMed](#)]
26. Nomiya, K.; Miwa, M. Structural stability index of heteropoly- and isopoly-anions. *Polyhedron* **1984**, *3*, 341–346. [[CrossRef](#)]
27. Müller, A.; Krickemeyer, E.; Meyer, J.; Bögge, H.; Peters, F.; Plass, W.; Diemann, E.; Dillinger, S.; Nonnenbruch, F.; Randerath, M.; et al. $[Mo_{154}(NO)_{14}O_{420}(OH)_{28}(H_2O)_{70}]^{(25\pm 5)-}$: A Water-Soluble Big Wheel with More than 700 Atoms and a Relative Molecular Mass of About 24000. *Angew. Chem. Int. Ed. Engl.* **1995**, *34*, 2122–2124. [[CrossRef](#)]
28. Müller, A.; Krickemeyer, E.; Bögge, H.; Schmidtman, M.; Beugholt, C.; Kögerler, P.; Lu, C. Formation of a Ring-Shaped Reduced “Metal Oxide” with the Simple Composition $[(MoO_3)_{176}(H_2O)_{80}H_{32}]$. *Angew. Chem. Int. Ed.* **1998**, *37*, 1220–1223. [[CrossRef](#)]
29. Müller, A.; Krickemeyer, E.; Bögge, H.; Schmidtman, M.; Peters, F. Organizational Forms of Matter: An Inorganic Super Fullerene and Keplerate Based on Molybdenum Oxide. *Angew. Chem. Int. Ed.* **1998**, *37*, 3359–3363. [[CrossRef](#)]
30. Chilas, G.I.; Miras, H.N.; Manos, M.J.; Woollins, J.D.; Slawin, A.M.Z.; Stylianou, M.; Keramidias, A.D.; Kabanos, T.A. Oxovanadium(IV)-sulfite compounds: Synthesis and structural and physical studies. *Pure Appl. Chem.* **2005**, *77*, 1529–1538. [[CrossRef](#)]
31. Miras, H.N.; Stone, D.J.; McInnes, E.J.L.; Raptis, R.G.; Baran, P.; Chilas, G.I.; Sigalas, M.P.; Kabanos, T.A.; Cronin, L. Solution identification and solid state characterisation of a heterometallic polyoxometalate $\{Mo_{11}V_7\}$: $[Mo^VI_{11}V^V_5V^{IV}_2O_{52}(\mu_9-SO_3)]^{7-}$. *Chem. Commun. (Camb.)* **2008**, *52*, 4703–4705. [[CrossRef](#)] [[PubMed](#)]

32. Sartzi, H.; Long, D.-L.; Sproules, S.; Cronin, L.; Miras, H.N. Directed Self-Assembly, Symmetry Breaking, and Electronic Modulation of Metal Oxide Clusters by Pyramidal Heteroanions. *Chem. A Eur. J.* **2018**, *24*, 4399–4411. [[CrossRef](#)] [[PubMed](#)]
33. Finke, R.G.; Rapko, B.; Saxton, R.J.; Domaille, P.J. Trisubstituted heteropolytungstates as soluble metal oxide analogs. III. Synthesis, characterization, phosphorus-31, silicon-29, vanadium-51, and 1- and 2-D tungsten-183 NMR, deprotonation, and proton mobility studies of organic solvent solute forms of $H_xSiW_9V_3O_{40}^{x-7}$ and $H_xP_2W_{15}V_3O_{62}^{x-9}$. *J. Am. Chem. Soc.* **1986**, *108*, 2947–2960. [[CrossRef](#)]
34. Finke, R.G.; Lyon, D.K.; Nomiya, K.; Weakley, T.J.R. Structure of nonasodium α -triniobatopentadecawolframatodiphosphate–acetonitrile–water (1/2/23), $Na_9[P_2W_{15}Nb_3O_{62}] \cdot 2CH_3CN \cdot 23H_2O$. *Acta Crystallogr. Sect. C Cryst. Struct. Commun.* **1990**, *46*, 1592–1596. [[CrossRef](#)]
35. Sakai, Y.; Kitakoga, Y.; Hayashi, K.; Yoza, K.; Nomiya, K. Isolation and Molecular Structure of a Monomeric, Tris[peroxotitanium(IV)]-Substituted α -Dawson Polyoxometalate Derived from the Tetrameric Anhydride Form Composed of Four Tris[titanium(IV)]-Substituted α -Dawson Substructures and Four Bridging Titanium(IV) Octahedral Groups. *Eur. J. Inorg. Chem.* **2004**, *2004*, 4646–4652. [[CrossRef](#)]
36. Finke, R.G.; Droege, M.W. Trivalent heteropolytungstate derivatives. 2. Synthesis, characterization, and tungsten-183 NMR of $P_4W_{30}M_4(H_2O)_2O_{112}^{16-}$ (M = Co, Cu, Zn). *Inorg. Chem.* **1983**, *22*, 1006–1008. [[CrossRef](#)]
37. Gomez-Garcia, C.J.; Borrás-Almenar, J.J.; Coronado, E.; Ouahab, L. Single-Crystal X-ray Structure and Magnetic Properties of the Polyoxotungstate Complexes $Na_{16}[M_4(H_2O)_2(P_2W_{15}O_{56})_2] \cdot nH_2O$ (M = Mn^{II} , $n = 53$; M = Ni^{II} , $n = 52$): An Antiferromagnetic Mn^{II} Tetramer and a Ferromagnetic Ni^{II} Tetramer. *Inorg. Chem.* **1994**, *33*, 4016–4022. [[CrossRef](#)]
38. Zhang, X.; Chen, Q.; Duncan, D.C.; Campana, C.F.; Hill, C.L. Multiiron Polyoxoanions. Syntheses, Characterization, X-ray Crystal Structures, and Catalysis of H_2O_2 -Based Hydrocarbon Oxidations by $[Fe^{III}_4(H_2O)_2(P_2W_{15}O_{56})_2]^{12-}$. *Inorg. Chem.* **1997**, *36*, 4208–4215. [[CrossRef](#)]
39. Weakley, T.J.R.; Finke, R.G. Single-crystal X-ray structures of the polyoxotungstate salts $K_{8.3}Na_{1.7}[Cu_4(H_2O)_2(PW_9O_{34})_2] \cdot 24H_2O$ and $Na_{14}Cu[Cu_4(H_2O)_2(P_2W_{15}O_{56})_2] \cdot 53H_2O$. *Inorg. Chem.* **1990**, *29*, 1235–1241. [[CrossRef](#)]
40. Fang, X.; Kögerler, P. PO_4^{3-} -Mediated Polyoxometalate Supercluster Assembly. *Angew. Chem. Int. Ed.* **2008**, *47*, 8123–8126. [[CrossRef](#)] [[PubMed](#)]
41. Pradeep, C.P.; Long, D.-L.; Kögerler, P.; Cronin, L. Controlled assembly and solution observation of a 2.6 nm polyoxometalate ‘super’ tetrahedron cluster: $[KFe_{12}(OH)_{18}(\alpha-1,2,3-P_2W_{15}O_{56})_4]^{29-}$. *Chem. Commun.* **2007**, 4254–4256. [[CrossRef](#)]
42. Sakai, Y.; Yoshida, S.; Hasegawa, T.; Murakami, H.; Nomiya, K. Tetrameric, Tri-Titanium(IV)-Substituted Polyoxometalates with an α -Dawson Substructure as Soluble Metal Oxide Analogues. Synthesis and Molecular Structure of Three Giant “Tetrapods” Encapsulating Different Anions (Br^- , I^- , and NO_3^-). *Bull. Chem. Soc. Jpn.* **2007**, *80*, 1965–1974. [[CrossRef](#)]
43. Cadot, E.; Pilette, M.-A.; Marrot, J.; Sécheresse, F. A Supramolecular Tetra-Dawson Polyoxothiometalate: $[(\alpha-H_2P_2W_{15}O_{56})_4\{Mo_2O_2S_2(H_2O)_2\}_4\{Mo_4S_4O_4(OH)_2(H_2O)\}_2]^{28-}$. *Angew. Chem. Int. Ed.* **2003**, *42*, 2173–2176. [[CrossRef](#)] [[PubMed](#)]
44. Fang, X.; Kögerler, P.; Isaacs, L.; Uchida, S.; Mizuno, N. Cucurbit[n]uril-Polyoxoanion Hybrids. *J. Am. Chem. Soc.* **2009**, *131*, 432–433. [[CrossRef](#)] [[PubMed](#)]
45. Cao, H.-L.; Cai, F.-Y.; Huang, H.-B.; Karadeniz, B.; Lü, J. Polyoxometalate-cucurbituril molecular solid as photocatalyst for dye degradation under visible light. *Inorg. Chem. Commun.* **2017**, *84*, 164–167. [[CrossRef](#)]
46. Zou, C.; Zhao, P.; Ge, J.; Qin, Y.; Luo, P. Oxidation/adsorption desulfurization of natural gas by bridged cyclodextrins dimer encapsulating polyoxometalate. *Fuel* **2013**, *104*, 635–640. [[CrossRef](#)]
47. Wu, Y.; Shi, R.; Wu, Y.-L.; Holcroft, J.M.; Liu, Z.; Frascioni, M.; Wasielewski, M.R.; Li, H.; Stoddart, J.F. Complexation of Polyoxometalates with Cyclodextrins. *J. Am. Chem. Soc.* **2015**, *137*, 4111–4118. [[CrossRef](#)] [[PubMed](#)]
48. Moussawi, M.A.; Leclerc-Laronze, N.; Floquet, S.; Abramov, P.A.; Sokolov, M.N.; Cordier, S.; Ponchel, A.; Monflier, E.; Bricout, H.; Landy, D.; et al. Polyoxometalate, Cationic Cluster, and γ -Cyclodextrin: From Primary Interactions to Supramolecular Hybrid Materials. *J. Am. Chem. Soc.* **2017**, *139*, 12793–12803. [[CrossRef](#)] [[PubMed](#)]

49. Moussawi, M.A.; Haouas, M.; Floquet, S.; Shepard, W.E.; Abramov, P.A.; Sokolov, M.N.; Fedin, V.P.; Cordier, S.; Ponchel, A.; Monflier, E.; et al. Nonconventional Three-Component Hierarchical Host–Guest Assembly Based on Mo-Blue Ring-Shaped Giant Anion, γ -Cyclodextrin, and Dawson-type Polyoxometalate. *J. Am. Chem. Soc.* **2017**, *139*, 14376–14379. [[CrossRef](#)] [[PubMed](#)]
50. Miras, H.N.; Vilà-Nadal, L.; Cronin, L. Polyoxometalate based open-frameworks (POM-OFs). *Chem. Soc. Rev.* **2014**, *43*, 5679–5699. [[CrossRef](#)] [[PubMed](#)]
51. An, H.; Hou, Y.; Wang, L.; Zhang, Y.; Yang, W.; Chang, S. Evans–Showell-Type Polyoxometalates Constructing High-Dimensional Inorganic–Organic Hybrid Compounds with Copper–Organic Coordination Complexes: Synthesis and Oxidation Catalysis. *Inorg. Chem.* **2017**, *56*, 11619–11632. [[CrossRef](#)] [[PubMed](#)]
52. Wang, X.; Sun, J.; Lin, H.; Chang, Z.; Wang, X.; Liu, G. A series of Anderson-type polyoxometalate-based metal–organic complexes: Their pH-dependent electrochemical behaviour, and as electrocatalysts and photocatalysts. *Dalton Trans.* **2016**, *45*, 12465–12478. [[CrossRef](#)] [[PubMed](#)]
53. Lan, Y.-Q.; Li, S.-L.; Wang, X.-L.; Shao, K.-Z.; Du, D.-Y.; Zang, H.-Y.; Su, Z.-M. Self-Assembly of Polyoxometalate-Based Metal Organic Frameworks Based on Octamolybdates and Copper–Organic Units: From Cu^{II} , $\text{Cu}^{\text{I,II}}$ to Cu^{I} via Changing Organic Amine. *Inorg. Chem.* **2008**, *47*, 8179–8187. [[CrossRef](#)] [[PubMed](#)]
54. Koo, B.-K.; Bewley, L.; Golub, V.; Rarig, R.S.; Burkholder, E.; O’Connor, C.J.; Zubieta, J. Anion influences on the construction of one-dimensional structures of the Cu(II)–bisterpy family (bisterpy = 2,2':4',4'':2'',2'''-quarterpyridyl, 6',6''-di-2-pyridiine). *Inorg. Chim. Acta* **2003**, *351*, 167–176. [[CrossRef](#)]
55. Su, Z.-H.; Zhou, B.-B.; Zhao, Z.-F.; Zhang, X. A novel 1D chain compound constructed from copper-complex fragments-substituted dilacunary β -octamolybdate units and saturated β -octamolybdate clusters. *Inorg. Chem. Commun.* **2008**, *11*, 334–337. [[CrossRef](#)]
56. Li, S.-L.; Lan, Y.-Q.; Ma, J.-F.; Yang, J.; Wang, X.-H.; Su, Z.-M. Syntheses and Structures of Organic-Inorganic Hybrid Compounds Based on Metal-Fluconazole Coordination Polymers and the β - Mo_8O_{26} Anion. *Inorg. Chem.* **2007**, *46*, 8283–8290. [[CrossRef](#)] [[PubMed](#)]
57. Abbas, H.; Streb, C.; Pickering, A.L.; Neil, A.R.; Long, D.-L.; Cronin, L. Molecular Growth of Polyoxometalate Architectures Based on $[-\text{Ag}\{\text{Mo}_8\}\text{Ag}-]$ Synthons: Toward Designed Cluster Assemblies. *Cryst. Growth Des.* **2008**, *8*, 635–642. [[CrossRef](#)]
58. Abbas, H.; Pickering, A.L.; Long, D.-L.; Kögerler, P.; Cronin, L. Controllable Growth of Chains and Grids from Polyoxomolybdate Building Blocks Linked by Silver(I) Dimers. *Chem. A Eur. J.* **2005**, *11*, 1071–1078. [[CrossRef](#)] [[PubMed](#)]
59. Dolbecq, A.; Mialane, P.; Sécheresse, F.; Keita, B.; Nadjjo, L. Functionalized polyoxometalates with covalently linked bisphosphonate, N-donor or carboxylate ligands: From electrocatalytic to optical properties. *Chem. Commun.* **2012**, *48*, 8299–8316. [[CrossRef](#)] [[PubMed](#)]
60. Mirzaei, M.; Eshtiagh-Hosseini, H.; Nikpour, M.; Gholizadeh, A.; Ebrahimi, A. Synthesis, X-ray Crystal Structure and Spectroscopic Characterization of a Hybrid Material Based on Glycine and α -Keggin Type Polyoxotungstate. *Mendeleev Commun.* **2012**, *22*, 141–142. [[CrossRef](#)]
61. Eshtiagh-Hosseini, H.; Mirzaei, M. Two Novel Chiral Inorganic–Organic Hybrid Materials Containing Preyssler and Wells–Dawson Heteropolyoxometallates with Valine (val), Glycine (gly), and Proline (pro) Amino acids: $(\text{Hval})_2(\text{Hgly})(\text{H}_3\text{O})_6\text{K}_5[\text{Na}(\text{H}_2\text{O})\text{P}_5\text{W}_{30}\text{O}_{110}] \cdot 19.5\text{H}_2\text{O}$ and $(\text{Hpro})_6[\text{P}_2\text{W}_{18}\text{O}_{62}] \cdot 8\text{H}_2\text{O}$. *J. Clust. Sci.* **2012**, *23*, 345–355. [[CrossRef](#)]
62. Compain, J.-D.; Mialane, P.; Marrot, J.; Sécheresse, F.; Zhu, W.; Oldfield, E.; Dolbecq, A. Tetra- to Dodecanuclear Oxomolybdate Complexes with Functionalized Bisphosphonate Ligands: Activity in Killing Tumor Cells. *Chem. A Eur. J.* **2010**, *16*, 13741–13748. [[CrossRef](#)] [[PubMed](#)]
63. Sarafianos, S.G.; Kortz, U.; Pope, M.T.; Modak, M.J. Mechanism of polyoxometalate-mediated inactivation of DNA polymerases: An analysis with HIV-1 reverse transcriptase indicates specificity for the DNA-binding cleft. *Biochem. J.* **1996**, *319*, 619–626. [[CrossRef](#)] [[PubMed](#)]
64. Rhule, J.T.; Hill, C.L.; Judd, D.A.; Schinazi, R.F. Polyoxometalates in Medicine. *Chem. Rev.* **1998**, *98*, 327–358. [[CrossRef](#)] [[PubMed](#)]
65. Hasenknopf, B. Polyoxometalates: Introduction to a class of inorganic compounds and their biomedical applications. *Front. Biosci.* **2005**. [[CrossRef](#)]

66. Molitor, C.; Bijelic, A.; Rompel, A. In situ formation of the first proteinogenically functionalized $[\text{TeW}_6\text{O}_{24}\text{O}_2(\text{Glu})]^{7-}$ structure reveals unprecedented chemical and geometrical features of the Anderson-type cluster. *Chem. Commun.* **2016**, *52*, 12286–12289. [[CrossRef](#)] [[PubMed](#)]
67. Fu, L.; Gao, H.; Yan, M.; Li, S.; Li, X.; Dai, Z.; Liu, S. Polyoxometalate-Based Organic–Inorganic Hybrids as Antitumor Drugs. *Small* **2015**, *11*, 2938–2945. [[CrossRef](#)] [[PubMed](#)]
68. Xue, Z.; Jiang, J.; Li, M.; Mu, T. Gadolinium-Based Metal–Organic Framework as an Efficient and Heterogeneous Catalyst To Activate Epoxides for Cycloaddition of CO_2 and Alcoholysis. *ACS Sustain. Chem. Eng.* **2017**, *5*, 2623–2631. [[CrossRef](#)]
69. Sun, J.-W.; Yan, P.-F.; An, G.-H.; Sha, J.-Q.; Li, G.-M.; Yang, G.-Y. Immobilization of Polyoxometalate in the Metal–organic Framework rht-MOF-1: Towards a Highly Effective Heterogeneous Catalyst and Dye Scavenger. *Sci. Rep.* **2016**, *6*, 25595. [[CrossRef](#)] [[PubMed](#)]
70. Nohra, B.; El Moll, H.; Rodriguez Albelo, L.M.; Mialane, P.; Marrot, J.; Mellot-Draznieks, C.; O’Keeffe, M.; Ngo Biboum, R.; Lemaire, J.; Keita, B.; et al. Polyoxometalate-Based Metal Organic Frameworks (POMOFs): Structural Trends, Energetics, and High Electrocatalytic Efficiency for Hydrogen Evolution Reaction. *J. Am. Chem. Soc.* **2011**, *133*, 13363–13374. [[CrossRef](#)] [[PubMed](#)]
71. Mitchell, S.G.; Streb, C.; Miras, H.N.; Boyd, T.; Long, D.-L.; Cronin, L. Face-directed self-assembly of an electronically active Archimedean polyoxometalate architecture. *Nat. Chem.* **2010**, *2*, 308–312. [[CrossRef](#)] [[PubMed](#)]
72. Zhang, H.-L.; Liao, J.-Z.; Yang, W.; Wu, X.-Y.; Lu, C.-Z. A novel naphthalenediimide-based lanthanide–organic framework with polyoxometalate templates exhibiting reversible photochromism. *Dalton Trans.* **2017**, *46*, 4898–4901. [[CrossRef](#)] [[PubMed](#)]
73. Yaghi, O.M.; Li, H. Hydrothermal Synthesis of a Metal–organic Framework Containing Large Rectangular Channels. *J. Am. Chem. Soc.* **1995**, *117*, 10401–10402. [[CrossRef](#)]
74. Chen, T.-H.; Popov, I.; Kaveevivitchai, W.; Miljanić, O.Š. Metal–Organic Frameworks: Rise of the Ligands. *Chem. Mater.* **2014**, *26*, 4322–4325. [[CrossRef](#)]
75. Zhou, H.-C.; Kitagawa, S. Metal–Organic Frameworks (MOFs). *Chem. Soc. Rev.* **2014**, *43*, 5415–5418. [[CrossRef](#)] [[PubMed](#)]
76. Zheng, B.; Bai, J.; Duan, J.; Wojtas, L.; Zaworotko, M.J. Enhanced CO_2 Binding Affinity of a High-Uptake rht-Type Metal–Organic Framework Decorated with Acylamide Groups. *J. Am. Chem. Soc.* **2011**, *133*, 748–751. [[CrossRef](#)] [[PubMed](#)]
77. Kondo, M.; Furukawa, S.; Hirai, K.; Kitagawa, S. Coordinatively Immobilized Monolayers on Porous Coordination Polymer Crystals. *Angew. Chem. Int. Ed.* **2010**, *49*, 5327–5330. [[CrossRef](#)] [[PubMed](#)]
78. Liu, J.; Chen, L.; Cui, H.; Zhang, J.; Zhang, L.; Su, C.-Y. Applications of metal–organic frameworks in heterogeneous supramolecular catalysis. *Chem. Soc. Rev.* **2014**, *43*, 6011–6061. [[CrossRef](#)] [[PubMed](#)]
79. Jang, M.-S.; Lee, Y.-R.; Ahn, W.-S. CO_2 Cycloaddition of Epichlorohydrin over NH_2 -Functionalized MIL-101. *Bull. Korean Chem. Soc.* **2015**, *36*, 363–366. [[CrossRef](#)]
80. Jeong, H.-M.; Roshan, R.; Babu, R.; Kim, H.-J.; Park, D.-W. Zirconium-based isoreticular metal–organic frameworks for CO_2 fixation via cyclic carbonate synthesis. *Korean J. Chem. Eng.* **2018**, *35*, 438–444. [[CrossRef](#)]
81. Li, H.; Wang, K.; Sun, Y.; Lollar, C.T.; Li, J.; Zhou, H.-C. Recent advances in gas storage and separation using metal–organic frameworks. *Mater. Today* **2018**, *21*, 108–121. [[CrossRef](#)]
82. Jiang, J.; Furukawa, H.; Zhang, Y.-B.; Yaghi, O.M. High Methane Storage Working Capacity in Metal–Organic Frameworks with Acrylate Links. *J. Am. Chem. Soc.* **2016**, *138*, 10244–10251. [[CrossRef](#)] [[PubMed](#)]
83. Zou, L.; Zhou, H.-C. Hydrogen Storage in Metal–organic Frameworks. In *Nanostructured Materials for Next-Generation Energy Storage and Conversion*; Springer: Berlin/Heidelberg, Germany, 2017; pp. 143–170.
84. Dey, C.; Kundu, T.; Biswal, B.P.; Mallick, A.; Banerjee, R. Crystalline metal–organic frameworks (MOFs): Synthesis, structure and function. *Acta Crystallogr. Sect. B* **2014**, *70*, 3–10. [[CrossRef](#)] [[PubMed](#)]
85. Al Haydar, M.; Abid, H.R.; Sunderland, B.; Wang, S. Metal organic frameworks as a drug delivery system for flurbiprofen. *Drug Des. Dev. Ther.* **2017**, *11*, 2685–2695. [[CrossRef](#)] [[PubMed](#)]
86. Sun, C.-Y.; Qin, C.; Wang, X.-L.; Su, Z.-M. Metal–organic frameworks as potential drug delivery systems. *Expert Opin. Drug Deliv.* **2013**, *10*, 89–101. [[CrossRef](#)] [[PubMed](#)]
87. Orellana-Tavra, C.; Marshall, R.J.; Baxter, E.F.; Abá, I.; Zaro, L.; Tao, A.; Cheetham, A.K.; Forgan, R.S.; Fairen-Jimenez, D. Drug delivery and controlled release from biocompatible metal–organic frameworks using mechanical amorphization. *J. Mater. Chem. B* **2016**, *4*, 7697–7707. [[CrossRef](#)]

88. Li, T.; Miras, H.N.; Song, Y.-F. Polyoxometalate (POM)-Layered Double Hydroxides (LDH) composite materials: Design and catalytic applications. *Catalysts* **2017**, *7*, 260. [[CrossRef](#)]
89. Chen, Y.; Yao, Z.; Miras, H.N.; Song, Y.-F. Modular Polyoxometalate-Layered Double Hydroxide Composites as Efficient Oxidative Catalysts. *Chem. A Eur. J.* **2015**, *21*. [[CrossRef](#)] [[PubMed](#)]
90. Xu, Y.; Xuan, W.; Zhang, M.; Miras, H.N.; Song, Y.-F. A multicomponent assembly approach for the design of deep desulfurization heterogeneous catalysts. *Dalton Trans.* **2016**, *45*. [[CrossRef](#)] [[PubMed](#)]
91. Liu, K.; Yao, Z.; Miras, H.N.; Song, Y.-F. Facile Immobilization of a Lewis Acid Polyoxometalate onto Layered Double Hydroxides for Highly Efficient N-Oxidation of Pyridine-Based Derivatives and Denitrogenation. *ChemCatChem* **2015**, *7*. [[CrossRef](#)]
92. Li, T.; Wang, Z.; Chen, W.; Miras, H.N.; Song, Y.F. Rational Design of a Polyoxometalate Intercalated Layered Double Hydroxide: Highly Efficient Catalytic Epoxidation of Allylic Alcohols under Mild and Solvent-Free Conditions. *Chem. A Eur. J.* **2017**, *23*, 1069–1077. [[CrossRef](#)] [[PubMed](#)]
93. Kang, Z.; Fan, L.; Sun, D. Recent advances and challenges of metal–organic framework membranes for gas separation. *J. Mater. Chem. A* **2017**, *5*, 10073–10091. [[CrossRef](#)]
94. Zhao, Z.; Ma, X.; Kasik, A.; Li, Z.; Lin, Y.S. Gas Separation Properties of Metal Organic Framework (MOF-5) Membranes. *Ind. Eng. Chem. Res.* **2013**, *52*, 1102–1108. [[CrossRef](#)]
95. Liu, Y.; Wang, N.; Diestel, L.; Steinbach, F.; Caro, J. MOF membrane synthesis in the confined space of a vertically aligned LDH network. *Chem. Commun.* **2014**, *50*, 4225. [[CrossRef](#)] [[PubMed](#)]
96. Liu, P.-F.; Tao, K.; Li, G.-C.; Wu, M.-K.; Zhu, S.-R.; Yi, F.-Y.; Zhao, W.-N.; Han, L. In situ growth of ZIF-8 nanocrystals on layered double hydroxide nanosheets for enhanced CO₂ capture. *Dalton Trans.* **2016**, *45*, 12632–12635. [[CrossRef](#)] [[PubMed](#)]
97. Fujita, M.; Ogura, K. Supramolecular Self-Assembly of Macrocycles, Catenanes, and Cages through Coordination of Pyridine-Based Ligands to Transition Metals. *Bull. Chem. Soc. Jpn.* **1996**, *69*, 1471–1482. [[CrossRef](#)]
98. Cook, T.R.; Zheng, Y.-R.; Stang, P.J. Metal–Organic Frameworks and Self-Assembled Supramolecular Coordination Complexes: Comparing and Contrasting the Design, Synthesis, and Functionality of Metal–Organic Materials. *Chem. Rev.* **2013**, *113*, 734–777. [[CrossRef](#)] [[PubMed](#)]
99. Sun, Q.-F.; Iwasa, J.; Ogawa, D.; Ishido, Y.; Sato, S.; Ozeki, T.; Sei, Y.; Yamaguchi, K.; Fujita, M. Self-Assembled M₂₄L₄₈ Polyhedra and Their Sharp Structural Switch upon Subtle Ligand Variation. *Science* **2010**, *328*, 1144–1147. [[CrossRef](#)] [[PubMed](#)]
100. Chakrabarty, R.; Mukherjee, P.S.; Stang, P.J. Supramolecular Coordination: Self-Assembly of Finite Two- and Three-Dimensional Ensembles. *Chem. Rev.* **2011**, *111*, 6810–6918. [[CrossRef](#)] [[PubMed](#)]
101. Mukherjee, P.S.; Das, N.; Stang, P.J. Self-Assembly of Nanoscopic Coordination Cages Using a Flexible Tripodal Amide Containing Linker. *J. Org. Chem.* **2004**, *69*, 3526–3529. [[CrossRef](#)] [[PubMed](#)]
102. Castilla, A.M.; Ramsay, W.J.; Nitschke, J.R. Stereochemistry in Subcomponent Self-Assembly. *Acc. Chem. Res.* **2014**, *47*, 2063–2073. [[CrossRef](#)] [[PubMed](#)]
103. Brown, C.J.; Toste, F.D.; Bergman, R.G.; Raymond, K.N. Supramolecular Catalysis in Metal-Ligand Cluster Hosts. *Chem. Rev.* **2015**, *115*, 3012–3035. [[CrossRef](#)] [[PubMed](#)]
104. Howlader, P.; Das, P.; Zangrando, E.; Mukherjee, P.S. Urea-Functionalized Self-Assembled Molecular Prism for Heterogeneous Catalysis in Water. *J. Am. Chem. Soc.* **2016**, *138*, 1668–1676. [[CrossRef](#)] [[PubMed](#)]
105. Mal, P.; Breiner, B.; Rissanen, K.; Nitschke, J.R. White phosphorus is air-stable within a self-assembled tetrahedral capsule. *Science* **2009**, *324*, 1697–1699. [[CrossRef](#)] [[PubMed](#)]
106. Zhang, D.; Martinez, A.; Dutasta, J.-P. Emergence of Hemicryptophanes: From Synthesis to Applications for Recognition, Molecular Machines, and Supramolecular Catalysis. *Chem. Rev.* **2017**, *117*, 4900–4942. [[CrossRef](#)] [[PubMed](#)]
107. Rizzuto, F.J.; Wu, W.-Y.; Ronson, T.K.; Nitschke, J.R. Peripheral Templatation Generates an M^{II}₆L₄ Guest-Binding Capsule. *Angew. Chem. Int. Ed.* **2016**, *55*, 7958–7962. [[CrossRef](#)] [[PubMed](#)]
108. Catti, L.; Zhang, Q.; Tiefenbacher, K. Advantages of Catalysis in Self-Assembled Molecular Capsules. *Chem. A Eur. J.* **2016**, *22*, 9060–9066. [[CrossRef](#)] [[PubMed](#)]
109. Horiuchi, S.; Murase, T.; Fujita, M. Noncovalent Trapping and Stabilization of Dinuclear Ruthenium Complexes within a Coordination Cage. *J. Am. Chem. Soc.* **2011**, *133*, 12445–12447. [[CrossRef](#)] [[PubMed](#)]
110. Horiuchi, S.; Murase, T.; Fujita, M. A Remarkable Organometallic Transformation on a Cage-Incarcerated Dinuclear Ruthenium Complex. *Angew. Chem. Int. Ed.* **2012**, *51*, 12029–12031. [[CrossRef](#)] [[PubMed](#)]

111. Vajpayee, V.; Song, Y.H.; Jung, Y.J.; Kang, S.C.; Kim, H.; Kim, I.S.; Wang, M.; Cook, T.R.; Stang, P.J.; Chi, K.-W. Coordination-driven self-assembly of ruthenium-based molecular-rectangles: Synthesis, characterization, photo-physical and anticancer potency studies. *Dalton Trans.* **2012**, *41*, 3046–3052. [[CrossRef](#)] [[PubMed](#)]
112. Vajpayee, V.; Kim, H.; Mishra, A.; Mukherjee, P.S.; Stang, P.J.; Lee, M.H.; Kim, H.K.; Chi, K.-W. Self-assembled molecular squares containing metal-based donor: Synthesis and application in the sensing of nitro-aromatics. *Dalton Trans.* **2011**, *40*, 3112–3115. [[CrossRef](#)] [[PubMed](#)]
113. Sanz, S.; O'Connor, H.M.; Comar, P.; Baldansuren, A.; Pitak, M.B.; Coles, S.J.; Weihe, H.; Chilton, N.F.; McInnes, E.J.L.; Lusby, P.J.; et al. Modular $[\text{Fe}^{\text{III}}_8\text{M}^{\text{II}}_6]^{n+}$ ($\text{M}^{\text{II}} = \text{Pd}, \text{Co}, \text{Ni}, \text{Cu}$) Coordination Cages. *Inorg. Chem.* **2018**, *57*, 3500–3506. [[CrossRef](#)] [[PubMed](#)]
114. Sanz, S.; O'Connor, H.M.; Marti-Centelles, V.; Comar, P.; Pitak, M.B.; Coles, S.J.; Lorusso, G.; Palacios, E.; Evangelisti, M.; Baldansuren, A.; et al. $[\text{M}^{\text{III}}_2\text{M}^{\text{II}}_3]^{n+}$ trigonal bipyramidal cages based on diamagnetic and paramagnetic metalloligands. *Chem. Sci.* **2017**, *8*, 5526–5535. [[CrossRef](#)] [[PubMed](#)]
115. Zhao, C.; Toste, F.D.; Raymond, K.N.; Bergman, R.G. Nucleophilic Substitution Catalyzed by a Supramolecular Cavity Proceeds with Retention of Absolute Stereochemistry. *J. Am. Chem. Soc.* **2014**, *136*, 14409–14412. [[CrossRef](#)] [[PubMed](#)]
116. Qin, L.; Zhou, G.-J.; Yu, Y.-Z.; Nojiri, H.; Schröder, C.; Winpenny, R.E.P.; Zheng, Y.-Z. Topological Self-Assembly of Highly Symmetric Lanthanide Clusters: A Magnetic Study of Exchange-Coupling “Fingerprints” in Giant Gadolinium(III) Cages. *J. Am. Chem. Soc.* **2017**, *139*, 16405–16411. [[CrossRef](#)] [[PubMed](#)]
117. Boulon, M.-E.; Fernandez, A.; Moreno Pineda, E.; Chilton, N.F.; Timco, G.; Fielding, A.J.; Winpenny, R.E.P. Measuring Spin Spin Interactions between Heterospins in a Hybrid [2]Rotaxane. *Angew. Chem. Int. Ed.* **2017**, *56*, 3876–3879. [[CrossRef](#)] [[PubMed](#)]



© 2018 by the authors. Licensee MDPI, Basel, Switzerland. This article is an open access article distributed under the terms and conditions of the Creative Commons Attribution (CC BY) license (<http://creativecommons.org/licenses/by/4.0/>).